

THE M31 MICROLENSING EVENT WECAPP-GL1/POINT-AGAPE-S3: EVIDENCE FOR A MACHO COMPONENT IN THE DARK HALO OF M31?

A. RIFFESER¹, S. SEITZ^{1,2} AND R. BENDER^{1,2}

University Observatory Munich, Scheinerstrasse 1, 81679 München, Germany and
 Max Planck Institute for Extraterrestrial Physics, Giessenbachstrasse, 85748 Garching, Germany
Draft version October 31, 2018

ABSTRACT

We re-analyze the M31 microlensing event WeCAPP-GL1/Point-AGAPE-S3 taking into account that stars are not point-like but extended. We show that the finite size of stars can dramatically change the self-lensing event rate and (less dramatically) also the halo lensing event rate, if events are as bright as WeCAPP-GL1. The brightness of the brightest events mostly depends on the source sizes and fluxes and on the distance distribution of sources and lenses and therefore can be used as a sensitive discriminator between halo-lensing and self-lensing events, provided the stellar population mix of source stars is known well enough. Using a realistic model for the 3D-light distribution, stellar population and extinction of M31, we show that an event like WeCAPP-GL1 is very unlikely to be caused by self-lensing. In the entire WeCAPP-field ($17.2' \times 17.2'$ centered on the bulge) we expect only one self-lensing event every 49 years with the approximate parameters of WeCAPP-GL1 (full-width-half-maximum (FWHM) time-scale between 1 and 3 days and a flux excess of 19.0 mag or larger in R). On the other hand, if we assume only 20% of the dark halos of M31 and the Milky-Way consist of 1 solar mass MACHOs (Massive Astrophysical Compact Halo Objects) an event like WeCAPP-GL1 would occur every 10 years. Further more, if one uses position, FWHM time scale, flux excess and color of WeCAPP-GL1, self-lensing is even 13 times less likely than lensing by a MACHO, if MACHOs contribute 20% to the total halo mass and have masses in the range of 0.1 to 4 solar masses. We also demonstrate that (i) the brightness distribution of events in general is a good discriminator between self and halo lensing (ii) the time-scale distribution is a good discriminator if the MACHO mass is larger than 1 solar masses. Future surveys of M31 like PAndromeda (Pan-STARRS 1) should be able to provide many more such events within the next 4 years.

Subject headings: dark matter — gravitational lensing — galaxies: halos — galaxies: individual (M31, NGC 224) — Galaxy: halo — galaxies: luminosity function, mass function

1. INTRODUCTION

Microlensing searches towards Local Group galaxies are interesting in at least two respects. They can constrain the fraction of compact halo dark matter (MACHOs, see Paczyński (1986); Griest (1991)) and they allow to study stellar populations and the 3D distribution of stars in the Milky Way and the target galaxies. Lensing events caused by stars (self-lensing) also define a lower limit to the number of lensing events that have to be identified in a survey and therefore provide a consistency check for the lens model (depending on stellar population content, stellar dynamics and density distribution of the stars) and for the survey efficiency (see Alcock *et al.* (2001) for MACHO, and Tisserand *et al.* (2007); Afonso *et al.* (2003) for EROS and Calchi Novati *et al.* (2005) for POINT-AGAPE and de Jong *et al.* (2006) for MEGA). One can use the known characteristics of lensing and self lensing events to design surveys that will be dominated by self lensing. These self lensing-surveys can measure the faint end mass function of stellar populations (see Riffeser *et al.* (2006)).

One can obtain the most likely MACHO-mass fraction and its confidence limits from the analysis of all lensing events found in a survey (using number, spatial distribution, time scale distribution etc.) only after the selection criteria and the survey efficiency have been taken into account. The survey efficiency depends on the event characteristics (location, color, time scale and flux excess, finite source effects etc.) and on the sampling and photometric quality of observations. Including precise values for the survey efficiency can completely change the interpretation of a survey. Paulin-Henriksson & Calchi Novati (2004) concluded that there is no evidence for MACHOs towards M31 in the INT data set, whereas the same collaboration claimed with Calchi Novati *et al.* (2005) that there is a fairly strong evidence based on new efficiency estimates of the same survey.

Instead of comparing the expected and observed events one can analyze the observables of individual lensing events; these are flux excess at maximum magnification, full width half maximum time, color, location and presence/absence of finite source signatures in the light curve (see Riffeser *et al.* (2006) for more details). One can ask for the relative probability of halo lensing and self lensing and derive probability distributions for the lens masses causing that event. This has been done in a simplified way for WeCAPP-GL1 (Riffeser *et al.* (2003), or Paulin-Henriksson *et al.* (2003) for the POINT-AGAPE-S3 identification of the same event) and also for POINT-AGAPE N1 (Auriere *et al.* 2001) and

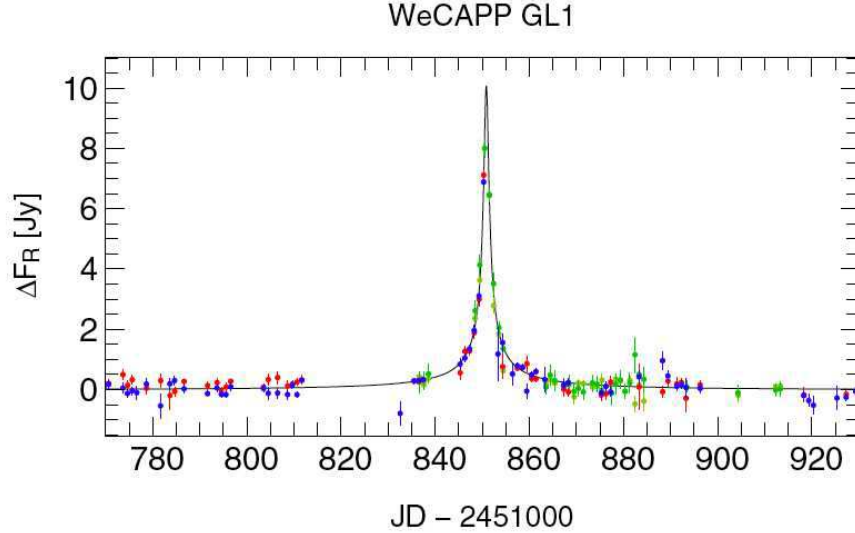


FIG. 1.— Light curve of WeCAPP GL1 (R band: blue, I band transformed to R band: red); POINT-AGAPE-S3 (r' band: dark green, i' band: light green)

N2 (An *et al.* 2004) in the past. However, the sources for all three events have been treated as point sources. This can mislead the interpretation, in particular if the events are very bright. This is also the case for light curves not showing any finite source signatures because the number of possible lens-source configurations strongly changes for bright events and the interpretation of the lens mass is modified.

It is the subject of our paper to (re)-analyze WeCAPP-GL1 and derive the relative probabilities of self lensing and halo lensing accounting for the extended sizes of stars. We summarize our M31 model in Appendix §A and present the equations needed for extended source stars in Appendix B and C. We demonstrate the pronounced differences resulting from this more accurate description of M31 in §2. In §3 we present the lens mass distribution without accounting for finite source effects and in §4 we show some qualitative results using the radius for the source stars. We evaluate in §5 an accurate estimate for the mass distribution of the event using the stellar source size. We investigate in §6 how sensitive the results are with respect to the mean M31 extinction and the line-of-sight (LOS) extinction towards WeCAPP-GL1 and in §7 with respect to the stellar population properties of the disk stars acting as sources. In §8 we give an outlook to the statistical interpretation for microlensing events in M31. Finally we draw our conclusions in §9.

2. AN IMPROVED WECAPP-GL1 ANALYSIS IN THE POINT SOURCE APPROXIMATION

For the current analysis we improve our light curve fit for WeCAPP-GL1 (Fig. 1) with respect to Riffeser *et al.* (2003), Table 2 by using a Paczyński microlensing light curve fit (5+2+2+2 free parameters in 4 filters; t_0 , u_0 , t_E , $F_{0,R}$, C_R , $F_{0,I}$, C_I , $F_{0,r'}$, $C_{r'}$, $F_{0,i'}$, $C_{i'}$) for the observables and a Gould microlensing function to determine the errors of the observables t_{FWHM} and ΔF . We also improved our photometric calibration accounting for the color terms in the filter calibration; our instrumental magnitudes \tilde{R} and \tilde{I} [phot/sec at AM=0] transform to the Johnson system with $R = \tilde{R} + 23.58 - 0.01(\tilde{R} - \tilde{I})$ and $I = \tilde{I} + 22.89 + 0.22(\tilde{R} - \tilde{I})$. The resulting parameters are listed in Table 1. Note that the fit implies that the source star of GL1 is a bright Red Giant Branch (RGB) star.

WeCAPP GL1	α (2000)	δ (2000)	t_0 (JD-2450000)	t_{FWHM} [d]	ΔF_R [10^{-5} Jy]	ΔF_I [10^{-5} Jy]	$(R - I)$ [mag]	A_0	\mathcal{M}_R [mag]	χ_{dof}
observables	00 ^h 42 ^m 30.28 ^s	41°13'01.1''	2451850.86	1.83	10.07	17.12	0.83	108	-0.64	1.33
error	$\pm 0.2''$	$\pm 0.2''$	± 0.02	± 0.10	± 0.44	± 0.78	± 0.03	± 57	-0.46/ + 0.82	

TABLE 1

SUMMARY OF WECAPP-GL1 (OR AGAPE-S3) OBSERVABLES (α AND δ) AND PARAMETERS DERIVED FROM A PACZYŃSKI MICROLENSING LIGHT CURVE FIT: DATE OF LIGHT CURVE MAXIMUM, FULL-WIDTH-HALF-MAXIMUM TIME t_{FWHM} OF THE EVENT, FLUX EXCESS AT LIGHT CURVE MAXIMUM IN R AND I-BAND, COLOR OF EVENT, QUALITY OF THE FIT, AND AN ESTIMATE FOR THE DEGENERATE AMPLIFICATION AND ABSOLUTE BRIGHTNESS OF THE SOURCE WITHOUT ERRORS.

Despite the well-sampled light curve of the event and the nicely fitting Paczyński light curve, finite source signatures above the highest data point of 8×10^{-5} Jy cannot be ruled out. Moreover, as we will demonstrate later on, finite source signatures for events brighter than 19 mag are indeed more likely than no finite source signatures. In a future work we are planning to use a modified light curve (see Riffeser *et al.* (2006), Eq. 12) that allows to include the finiteness of lenses and sources and their limb darkening.

The mass probability function for WeCAPP-GL1 was already derived in Riffeser *et al.* (2003) using a simplified analysis of the event and a simple description of M31.

We now use the improved analysis method derived in Riffeser *et al.* (2006) and a more detailed M31 model. We use

this M31 model for all calculations further on unless stated otherwise. The relevant differences for the analysis of WeCAPP-GL1 are as follows:

1. Color-magnitude relation of source stars

In Riffeser *et al.* (2003) we approximated the color-magnitude-relation $p_{\text{cmd},s}(\mathcal{M}, \mathcal{C})$ of bulge and disk stars in M31 with observations of M32 to derive a brightness estimate for a post main sequence star with a color of the WeCAPP-GL1 event. In this way, the brightness of a bulge star and a disk star with a color of WeCAPP-GL1 was estimated the same, $M_R = -1.5$ mag.

We now model the disk and bulge population separately, using the stellar population isochrones of Girardi *et al.* (2002) with a metallicity of $Z = Z_\odot$ (`isoc_z019.dat`). We describe the bulge as a 12.6 Gyr single stellar population (SSP).

The disk is modeled as a composite of 6 SSPs with ages of 4, 20, 100, 500 Myrs and 2.5 and 12.6 Gyrs. Their relative weights are calculated by integrating an exponentially declining star formation rate with $\tau = 8$ Gyrs over adjacent intervals (see Table 2). This simple model is close to a population where stars formed continuously over the past 12 Gyrs. In Figs. 2 and 3 we compare the luminosity and mass function of this composite stellar population with a population composed of 71 bursts with the same star formation decline rate of 8 Gyrs. The differences are marginal, i.e., our ‘simple’ model describes the brightness and mass distribution of stars with an e-folding timescale of 8 Gyrs fairly well, and offers the advantage of much faster numerical integrations in the color-magnitude plane.

age [Myr]	interval [Myr]	weight
4.0	0.0 - 12.0	0.00039
20.0	12.0 - 60.0	0.00158
100.0	60.0 - 300.6	0.00804
501.2	300.6 - 1506.5	0.04417
2511.9	1506.5 - 7550.6	0.35630
12589.3	7550.6 - 12589.3	0.58952

TABLE 2

The star formation history of M31 is not known exactly¹. Our choice ensures the presence of mostly old stars with a small fraction of young, blue and bright stars.

This implies that the stars in our model also populate the extremes of the M31-CMD (see Fig. 2).

We thus can allow for the effect that a few bright stars might be more efficient sources for detectable microlensing events than many fainter, older stars.

We now do not have to estimate the typical stellar brightness at a given color anymore, but can construct a brightness-color probability distribution $p_{\text{cmd}}(\mathcal{M}, \mathcal{C})$ from the isochrones and the assumed stellar mass function $\xi(M)$. The information provided in the Girardi isochrones also allows a straightforward extraction of the stellar radii $R_*(\mathcal{M}, \mathcal{C})$, which is necessary for an accurate treatment of finite-source size effects.

Note that the color information of the event helps to select a smaller set of sources and therefore the mass probability results from a smaller range of source brightness. Because of this additional information the mass probability distributions become narrower and more precise.

2. Analysis method

In Riffeser *et al.* (2003) we had estimated the approximate source brightness \mathcal{M} from the color of the event $\mathcal{C}^{\text{meas}}$, and derived a magnification A_0 to convert the observed full width half maximum time of the event $t_{\text{FWHM}}^{\text{meas}}$ to its Einstein-time scale $t_E \approx t_{\text{FWHM}}^{\text{meas}} / \sqrt{12} (A_0 - 1) \approx t_{\text{FWHM}}^{\text{meas}} / \sqrt{12} \Delta_F^{\text{meas}} / \{F_{\text{Vega}} 10^{-0.4[\mathcal{M}(p_{\text{cmd}}, \mathcal{C}^{\text{meas}}) + 24.43]}\}$. Using descriptions for bulge/disk/halo densities ρ and velocities p_{vt} , for the mass functions of stars $\xi(M)$ and a single mass MACHO halo we obtained the relative probabilities $p(M)$ for self lensing and halo lensing (as a function of the MACHO mass) with

$$p(M, t_E) \sim \xi(M) \int_0^\infty \rho_s(D_{\text{os}}) \int_0^{D_{\text{os}}} \rho_l(D_{\text{ol}}) p_{vt} \left(\frac{R_E}{t_E} \right) \left(\frac{R_E}{t_E} \right)^3 dD_{\text{ol}} dD_{\text{os}} \quad . \quad (1)$$

This means that the lens mass probability distribution $p(M, t_E)$ was obtained using the (unobservable) maximum magnification A_0 and Einstein-time t_E instead of the observables flux-excess Δ_F^{meas} and full-width half maximum time scale $t_{\text{FWHM}}^{\text{meas}}$.

¹ Brown *et al.* (2003)’s data and analysis suggest that (at least at a distance of 10 kpc where their data have been taken) about 30% percent of stars (in mass) could be as young as 6 – 8 Gyr. Also, the metallicity is large [see Mould & Kristian (1986), [M/H] = -0.6 Durrell *et al.* (1994), [Fe/H] = -0.6 Rich *et al.* (1996) [Fe/H] = -0.4] and falls off only at more than 30 kpc Kalirai *et al.* (2006).

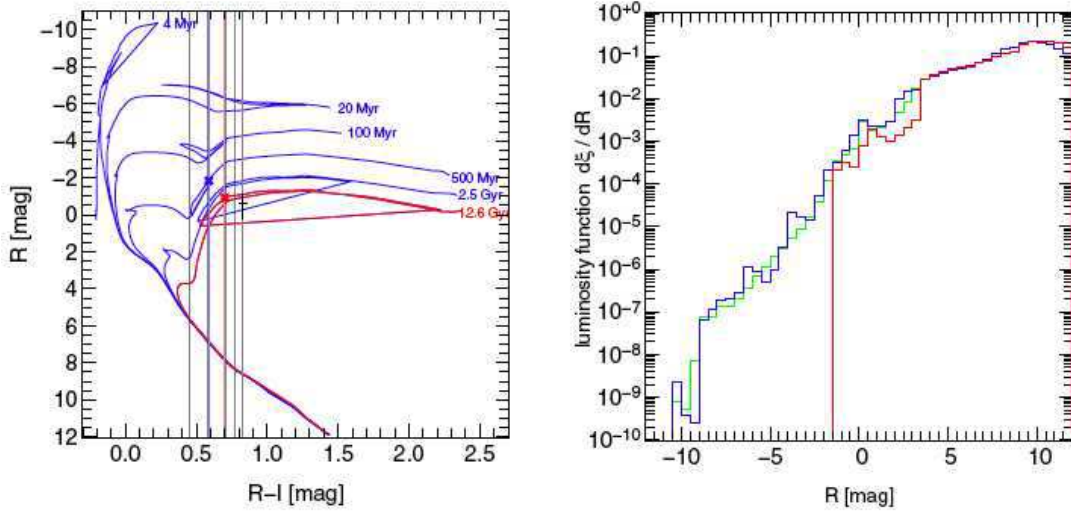


FIG. 2.— *Left panel:* Color ($R-I$) – R -band magnitude relations for stellar populations of the bulge (red) and disk components (blue) with solar metallicities (using isochrones of Girardi *et al.* (2002) in the Johnson filter system). *Right panel:* Luminosity function ξ for the bulge (red) and disk (blue) combining isochrones, weights and mass functions of our model. The green curve shows a nearly continuous disk population with 71 components.

We have shown in Riffeser *et al.* (2006) (Eqs. 80 and 84) that the Einstein-time–impact-parameter degeneracy leads to coupled errors for these two quantities, and thus should be avoided. In the following we will always use the real observables flux excess ΔF and time-scale t_{FWHM} instead of maximum magnification and Einstein time. Using the notation of Riffeser *et al.* (2006), the event rate per area, per event time scale t_{FWHM} , per flux excess ΔF , per source color \mathcal{C} , per absolute magnitude of the source star \mathcal{M} , and per lens mass M is

$$\frac{d^7\Gamma(x, y, t_{\text{FWHM}}, \Delta F, \mathcal{C}, M, \mathcal{M})}{dx dy dt_{\text{FWHM}} d\Delta F d\mathcal{C} dM d\mathcal{M}} = \frac{2 p_{\text{cmd}} \xi}{t_{\text{FWHM}}^3} \int_0^\infty n \left(\frac{\Psi}{F_0} \int_0^{D_{\text{ol}}^*} \rho R_E^3 p_{v_t}(v_t) dD_{\text{ol}} + \Omega^* \rho^* R_E^{*3} \int_0^{u_0^*} p_{v_t}(v_t^*) \Upsilon^{*2} du_0 \right) dD_{\text{os}} \quad (2)$$

All definitions are explained in Appendix B.

3. Mass function of stars

Riffeser *et al.* (2003) assumed that both disk and bulge stars are confined to a mass interval from $0.08M_\odot$ to $0.95M_\odot$ (bulge) and to $10M_\odot$ (disk) with a Zoccali *et al.* (2000) IMF ($\xi \sim M^{-1.33}$) for the bulge and a Gould *et al.* (1997) IMF for the disk, respectively. We now use those mass functions which are consistent with the stellar population models, i.e., a combination of a Ballero *et al.* (2007) & Kroupa (2002) IMF for the bulge and a Gould *et al.* (1997) & Kroupa (2002) IMF for the disk. Mass loss is provided by stellar population models (Girardi *et al.* 2002) and is taken into account in the mass function (MF).

We also extended the lower mass limits to $0.001M_\odot$.

Because of the small gradient of the MF for very small masses and their low cross section for microlensing all results are independent from the lower mass limit.

We also included stellar remnants originating at the high mass end of the IMF into the MF (see Renzini & Ciotti (1993)).

4. Extinction

In Riffeser *et al.* (2003) we did not account for the extinction along the line of sight to the source of the lensing event. Extinction alters the true color and brightness and thus the necessary magnification of a lensed source, which changes the shape of the mass probability function extracted from individual events.

The overall extinction decreases the observed flux, leading to the need to increase the number of stars (and thus the mass) to obtain the same luminosity.

Extinction in this way also influences the absolute and relative amplitudes of lensing and self lensing rates. The model of Riffeser *et al.* (2006) assumes an on average M31-extinction for all disk stars in the WeCAPP field of 0.51 mag and for all bulge stars of 0.19 mag in the R -band, independent of the angular position of the event, and independent of the LOS distance to the source. The MW-extinction is added uniformly with 0.17 mag (R -band).

With these assumptions on extinction one gets the following extincted colors for the bulge and disk stellar populations described above: for the bulge $(U-B)_{\text{meas}} = 0.78$, $(B-V)_{\text{meas}} = 1.19$, $(B-R)_{\text{meas}} = 1.91$, $(V-R)_{\text{meas}} = 0.72$, $(R-I)_{\text{meas}} = 0.75$, and for the disk $(U-B)_{\text{meas}} = -0.06$, $(B-V)_{\text{meas}} = 0.73$, $(B-R)_{\text{meas}} = 1.91$, $(V-R)_{\text{meas}} = 0.72$, $(R-I)_{\text{meas}} = 0.75$.

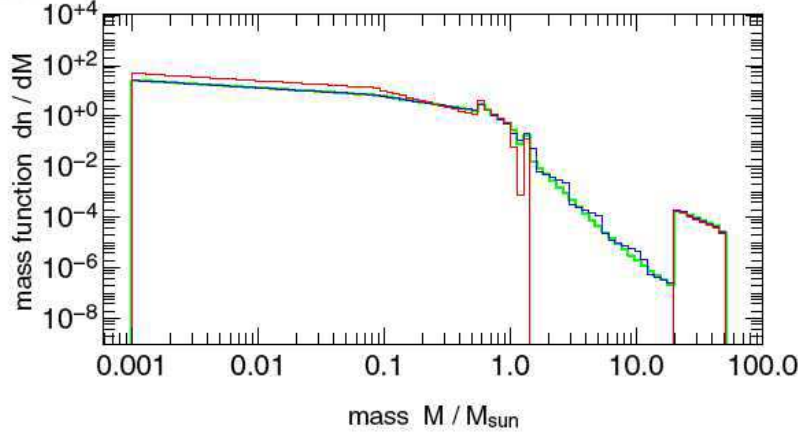


FIG. 3.— Present day mass function (MF) for M31 bulge (red) and disk (blue) population (mass loss according to Girardi *et al.* (2002)). Stars more massive than $1M_{\odot}$ are either young disk stars (blue) or disk/bulge stellar remnants (white dwarfs $\leq 1.13M_{\odot}$, neutron stars $\approx 1.4M_{\odot}$, black holes $\geq 20M_{\odot}$). The green curve shows a nearly continuous disk population with 71 components.

$R)_{\text{meas}} = 1.33$, $(V - R)_{\text{meas}} = 0.60$, $(R - I)_{\text{meas}} = 0.69$. Especially the values for the disk agree well with Waltherbos & Kennicutt (1987). We will use these extinction values if not specified otherwise. Additionally we use slightly refined extinction descriptions in § 6 later on.

5. Mass-to-light ratio (M/L) and total mass of bulge, disk and halo

Combining the luminosity function and the mass function results in the M/L ratios of $(M/L)_R = 3.3$ (bulge) and $(M/L)_R = 1.2$ (disk) not including extinction.

Using these (M/L) with the M31-light-model and the extinction assumptions results in a very similar massive bulge ($4.4 \times 10^{10}M_{\odot}$) and a more massive disk ($4.2 \times 10^{10}M_{\odot}$). Since we changed in particular the disk mass we now use a different halo model with a core radius of 5 kpc, a total mass of $1.23 \times 10^{12}M_{\odot}$, and a cut-off radius of 100 kpc. Note that the halo model has a large uncertainty since a large set of different combinations of core-radius, central-density, cut-off radius are able to fit the measured rotation curve of M31.

3. POINT SOURCE APPROXIMATION

In this section we present the lens mass distribution without accounting for finite source effects. We now demonstrate the impact of the change of assumptions described above on the interpretation of the event relative to Riffeser *et al.* (2003). In this chapter the sources are still treated as a point source.

The left panel of Figure 4 shows the lens mass distribution (event rate $\Gamma(M)$ per area, per event brightness ΔF , per event time scale t_{FWHM}) for WeCAPP-GL1 in the point source approximation using the LOS position ($x^{\text{meas}}, y^{\text{meas}}$), the time-scale ($t_{\text{FWHM}}^{\text{meas}}$), the flux-excess (ΔF^{meas}) and the color (C^{meas}) of the event and their errors. The assumptions in evaluating the event rates have been changed relative to Riffeser *et al.* (2003) as detailed in (1) to (5). The event rate for bulge-bulge lensing is 2 times as likely as bulge-disk lensing, about 13 times as likely as disk-bulge lensing and about 12 times as disk-disk lensing. For lensing of a bulge star by a $0.74M_{\odot}$ MACHO in M31 we obtained an event rate which is 12 times as likely as bulge-bulge self lensing. Using the event color the most likely halo lens masses for WeCAPP-GL1 are between $0.13M_{\odot}$ and $5.6M_{\odot}$. The main difference of this new analysis (still in the point source approximation!) relative to the result of Riffeser *et al.* (2003) is that the M31-halo-disk lensing scenario becomes now up to a factor 1/4 similar to the halo-bulge lensing (compared to Riffeser *et al.* (2003), where the M31-halo-bulge lensing was about 10 times as likely as halo-disk lensing). For the point source approximation the total halo-lensing contribution (summing over M31 and MW halo-bulge and halo-disk lensing) is 13 times more likely than all self lensing contributions.

In the right panel of Figure 4 we show the same calculations without using the color information of the event. At low masses the curves for $\Gamma(M)$ are only changed for disk sources, whereas bulge sources are not affected. The high mass end cut-off however is suppressed for all lens-source configurations due to the use of the measured event color. This is because the color of the WeCAPP-GL1 makes the source most efficient for becoming a very luminous event, and sources with colors different from WeCAPP-GL1 have smaller fluxes requiring larger Einstein radii and thus larger lens masses to achieve an event of the same brightness. Therefore, dropping the color information for WeCAPP-GL1 mainly affects the high mass probabilities.

In Fig. 5 we show the distribution of events in the ΔF - t_{FWHM} -plane in the point source approximation as obtained from Eq. C8 with location and intrinsic color of WeCAPP-GL1, $[(R - I)_0 = 0.59$ for disk sources, $(R - I)_0 = 0.70$ for bulge sources, without using its error]. Since in the point source approximation arbitrary large magnifications are possible, there is no limit for the brightness or shortness of the events. The event rate for events like WeCAPP-GL1 is equal for bulge-bulge and bulge-disk lensing. MACHO-lensing events caused by a $0.2M_{\odot}$ MACHO halo are roughly a factor of 10 more likely than self lensing for a full MACHO-halo.

Here the color information affected the shape of the event-rate contours in the t_{FWHM} - ΔF -plane. The ‘tilted M’-shape comes from the bimodal luminosity distribution of stars with color of WeCAPP-GL1: The luminosity function

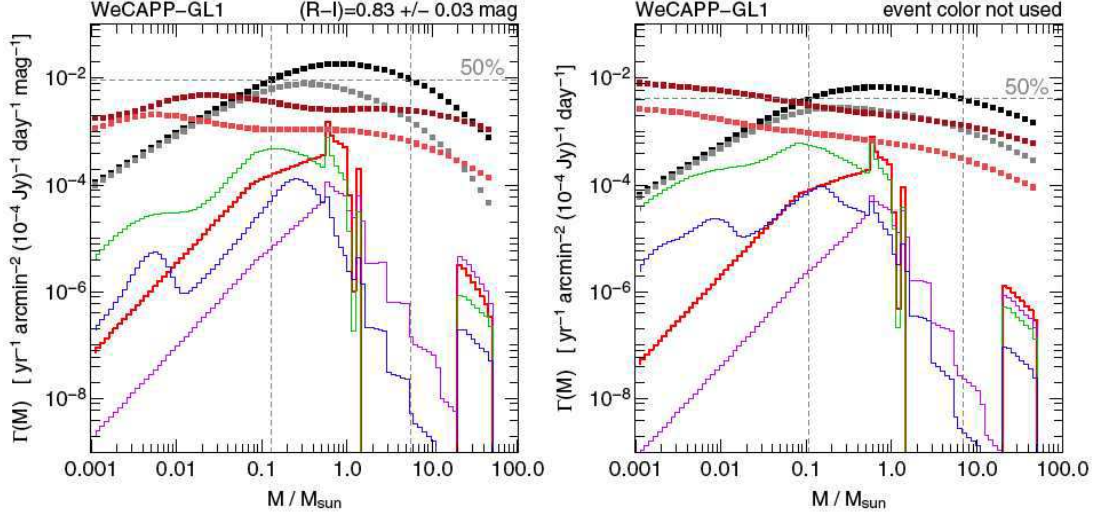


FIG. 4.— Lens mass distribution [event rate $\Gamma(M)$ per area, per event brightness ΔF , per event time scale t_{FWHM} , per color $(R-I)$] for WeCAPP-GL1 in the **point source approximation** using LOS position $(x^{\text{meas}}, y^{\text{meas}})$, time-scale $(t_{\text{FWHM}}^{\text{meas}})$, and flux-excess (Δ_F^{meas}) and their errors (Eq. C10). In the *left panel* the measured event color (C^{meas}) was transformed to the un-reddened color $(R-I)_0 = 0.59$ for disk sources, and $(R-I)_0 = 0.70$ for bulge sources, both with a Gaussian error of 0.03. The *right panel* was calculated not using the color information of the event. The *red, green, blue and purple* curves show the event rate for bulge-bulge, bulge-disk (bulge lens and disk source), disk-bulge and disk-disk lensing. The mass range is confined to the MF interval, and therefore there is an upper limit of about $50M_\odot$ resulting from black hole remnants. The amplitudes of the lens mass distributions are scaled such, that their maxima represent the expected rate due to the different lensing and self lensing scenarios and the ratios of their maxima yield the relative probabilities for the different scenarios. The information about halo lensing (M31-halo-bulge and M31-halo-disk data points are in *black* and *grey*, and MW-halo-bulge and MW-halo-disk in *brown* and *light-brown*) is displayed as points and not by a curve: we assume a mono-mass-spectrum for the halos, and each point represents a halo which is made of a given MACHO-mass to 100%. For each MACHO mass one obtains the event rate from the amplitude at that mass.

maps the magnification- t_{FWHM} -distribution into the ΔF space, see Eq. 62 in Riffeser *et al.* (2006). The color of the event constrains the luminosity of the post main sequence (PMS) sources fairly well, and one thus gets the ‘tilted M’-structure of the event rate in the ΔF - t_{FWHM} -plane. The left part is due to main sequence source stars, the right part due to PMS stars. Main sequence stars need larger magnification for the same event brightness, and since large magnification needs small impact parameters b , this goes in parallel with short FWHM-timescales, $t_{\text{FWHM}} \propto b/v_t$, of the events. If the PMS sources have a broader brightness distribution, the right part of the ‘M’ is washed out by moving it up and down vertically. Integrating over all colors makes the ‘M-shape’ almost disappear, since the width of the ‘M’ depends on the color (see Riffeser *et al.* (2006) for more details). Since the intrinsic color of WeCAPP-GL1 for bulge sources is between 0.6 and 0.8 (depending on the degree of reddening, see chapter 6), and the magnitude of the PMS-stars is fairly constant in this color range (see Fig. 2), the location of the right part of the ‘M’ is independent from color within the possible range of intrinsic colors of WeCAPP-GL1. The location of the event relative to the ‘tilted M’ provides an indication whether the time scale of the event fits to its brightness.

Figure 5 can also be used to visualize how plausible the observables ΔF - t_{FWHM} of an event candidate are. E.g., if MACHOs would have 100 solar masses, then for a given brightness of GL1, its timescale would be too low – or, on the other hand assuming GL1 is a convincing event, for MACHOs with $100M_\odot$ one would expect many more events with the same brightness but timescales of 10 days (which are not found).

To summarize in the point source approximation an event as bright as WeCAPP-GL1 is quite unlikely to be a self lensing event. The most likely self lensing scenario is bulge-bulge self lensing. The color information does only marginally influence the mass distributions. Noticeable is that for self-lensing low lens masses of $0.1M_\odot$ achieve relative high probabilities. Self-lensing is half as likely as halo-lensing, if MACHOs contribute 20% to the total halo mass and have a mass of about $1M_\odot$.

4. EFFECTS OF FINITE SOURCE SIZES: A QUALITATIVE UNDERSTANDING OF WECAPP-GL1

In this chapter we show for the fittings parameters of the source star (color $(R-I)_{\text{meas}} = 0.83$ and brightness $M_{\text{meas}} = -0.64$) that the lensing interpretation is strongly influenced by the finite-source treatment. Here we discuss the different competing effects qualitatively, while the full quantitative formalism is described in §5.

If a source is treated as point-like, it can be magnified at light curve maximum by a foreground point mass with any magnification value between one and infinity: for each Einstein-radius of a potential lens, there exists a source-lens-trajectory (an impact parameter) such that the desired magnification of the event can be achieved. However, if the source is extended, then the magnification at light curve maximum is no longer unlimited:

- if the impact parameter is larger than the projected source radius [$b > b^* \approx R_* D_{\text{ol}} / (2D_{\text{os}})$], nearly no finite source signatures appear in the event light curve, and all relations for the point source approximation hold.
- if the impact parameter is closer ($b < b^*$), the maximum magnification does only weakly depend on the impact parameter anymore. In our approximation (see Riffeser *et al.* (2006), Fig. 1) the maximum magnification depends

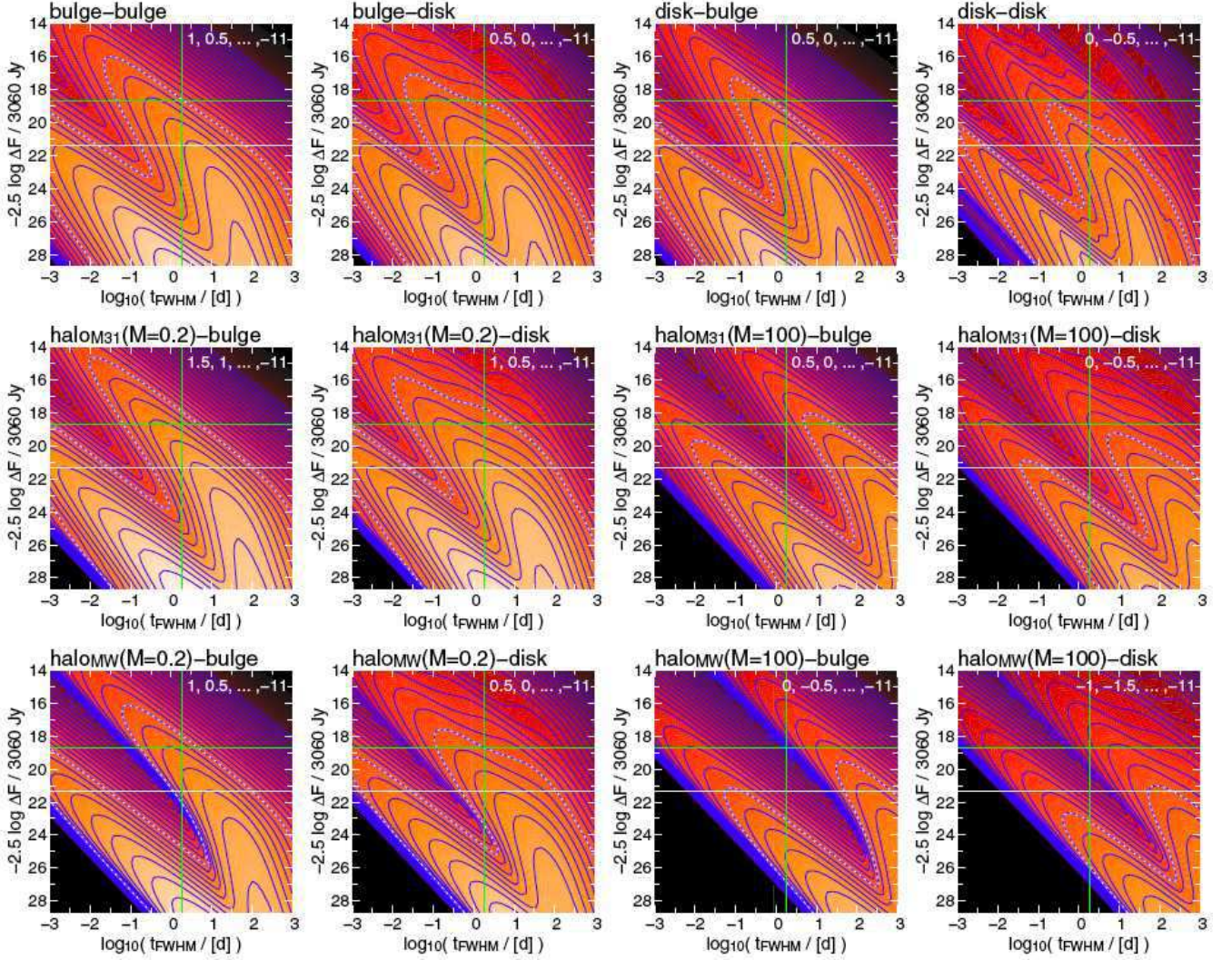


FIG. 5.— Contour plot of the time-scale and flux-excess distribution (ΔF - t_{FWHM} -plane) of events at the location and with the intrinsic color of WeCAPP-GL1, $[(R-I)_0 = 0.59$ for disk sources, $(R-I)_0 = 0.70$ for bulge sources, without using its error], obtained from Eq. C8 in the **point source approximation**. The first row shows self lensing, the second row M31 halo-lensing, the third row MW halo-lensing. The two further observables of WeCAPP-GL1 (flux excess and event time scale obtained from a point source lensing light curve fit) are marked in *green*. The estimate for the WeCAPP 6σ detection limit (see Riffeser *et al.* (2006), Table 1) at the position of GL1 is shown as *white line*. The contours differ by factors of $10^{0.5}$, and the dashed contour is that of 10^{-3} events per year, per square arc minute at the location of WeCAPP-GL1, per color (in magnitudes), per logarithmic timescale (time scale in days) and per flux-excess (converted to magnitudes) (see footnotes 3 and 2).

solely on the Einstein-radius and on the size of the source star, projected onto the lens plane, $R_* D_{\text{ol}}/D_{\text{os}}$ (see below, Eq. (3)). Therefore, for the highest magnifications there is no longer a trade-off between source-lens impact parameter b and Einstein-radius R_E , but between projected source size $R_* D_{\text{ol}}/D_{\text{os}}$ and Einstein-radius R_E . This means that the larger the projected source size is, the larger the Einstein-radius has to be to achieve a high magnification.

For self lensing, the Einstein-radii are limited by the maximum stellar masses (e.g. around $1M_\odot$ for the M31 bulge population) or the maximum remnant masses, the inefficient lensing geometries (fairly similar source D_{os} and lens distances D_{ol}), and large projected source radii. Therefore, high magnification events are hard to achieve. These effects are much less severe for halo lensing events. One therefore expects for bright lensing events that halo lensing becomes more likely relative to self lensing if the finite stellar sizes are taken into account. This could make the self lensing hypothesis for an event as bright as WeCAPP-GL1 very unlikely, although not completely un-feasible.

How easily an event can occur depends on the number of source-lens pairs that can produce the event. The LOS density distributions of bulge and disk are confined to a few kilo parsecs (see Fig. 6, left) which implies that the source-lens distances along the LOS must not be larger than a few kilo parsec for self lensing; otherwise either the source or the lens density and thus their product is small.

The relation between maximum magnification $A_0 = (\Delta F + F_0)/F_0 \approx \Delta F/F_0$, Einstein-radius R_E , and projected source radius $R_* D_{\text{ol}}/D_{\text{os}}$ is (Riffeser *et al.* (2006), Eq. (18))

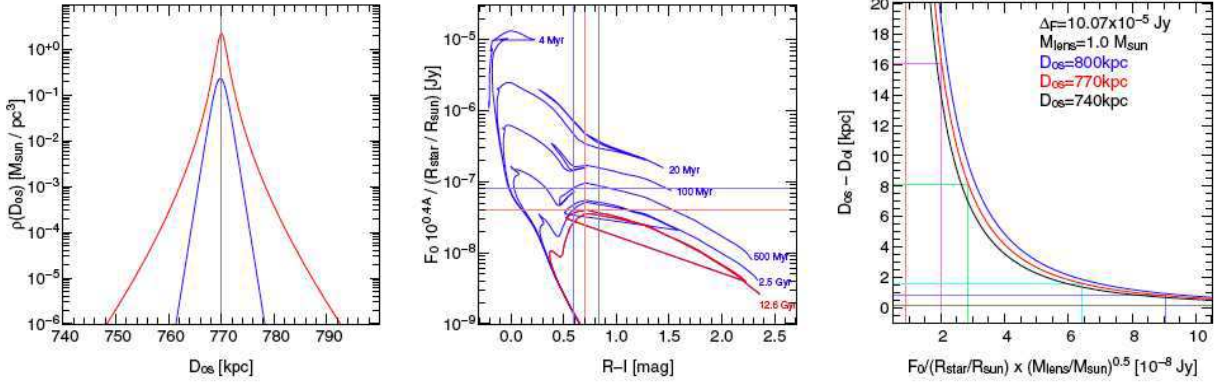


FIG. 6.— *Left panel* Density of bulge (red) and disk (blue) stars along the LOS to WeCAPP-GL1, using the M31-model described in Riffeser *et al.* (2006). In the *middle panel* we have transferred the stellar brightness to a flux (in Jansky's) at 770kpc (distance of M31), and obtained the ratio of this flux to the stellar size (in solar units). This ratio is an indicator of the maximum brightness of lensing events in the extended source description (see Eq. 3). *Right panel* Minimum distance that a source lens pair must have in order to cause an event as bright as WeCAPP-GL1 ($\Delta F_{\text{meas}} = 10.15 \times 10^{-5} \text{ Jy}$) as a function of the source characteristic (flux and radius) and lens mass. The *light red, magenta, green, cyan, blue, black* lines represent lenses with masses $0.1M_{\odot}, 0.5M_{\odot}, 1M_{\odot}, 5M_{\odot}, 10M_{\odot}$, and $50M_{\odot}$, respectively.

$$\Delta F_{\text{max}} = F_0 \left(\sqrt{1 + \frac{16GM D_{\text{os}}(D_{\text{os}} - D_{\text{ol}})}{c^2 R_*^2 D_{\text{ol}}}} - 1 \right) \approx \frac{4\sqrt{GM_{\odot}}}{R_{\odot}c} \sqrt{\frac{D_{\text{os}}(D_{\text{os}} - D_{\text{ol}})}{D_{\text{ol}}}} \frac{F_0 \sqrt{M/M_{\odot}}}{R_*/R_{\odot}} \approx 2F_0 \frac{R_E}{R_* \frac{D_{\text{ol}}}{D_{\text{os}}}}, \quad (3)$$

where the un-lensed source flux $F_0 = \text{flux}_R(\mathcal{M} + \mathcal{A})(10 \text{ pc}/D_{\text{os}})^2$ (see footnote 3) depends on the absolute source luminosity \mathcal{M} , the source distance D_{os} and the extinction \mathcal{A} towards the source. Note that our approximation Eq. 3 represents also the largest flux excess achievable by a light curve not showing finite source signatures.

Eq. 3 can be inverted to

$$D_{\text{ol,max}} \approx D_{\text{os}} \left(1 + \left(\frac{R_{\odot}c}{4\sqrt{GM_{\odot}}} \Delta F_{\text{max}} \frac{R_*/R_{\odot}}{F_0} \frac{1}{\sqrt{M/M_{\odot}}} \right)^2 \frac{1}{D_{\text{os}}} \right)^{-1}. \quad (4)$$

Eq. 4 provides the maximum distance a lens can have (to us) to allow a lensing event with a flux-excess ΔF_{max} at maximum magnification once the finite source sizes are taken into account. For a given source distance and a given source and lens population, the upper limit of that distance is set by the largest F_0/R_* -ratio for source stars and the largest lens mass possible. For a given (measured) flux excess of an event, Eq. (4) depends on the extinction along the line of sight: the smaller the extinction, the larger is ΔF_{max} ; also, the radii R_* have to be taken into account using the de-reddened color of the event. If the color information is available, one has to use the stellar radii of the de-reddened source to obtain the largest F_0/R_* - ratio for source stars.

In Fig. 6b (middle panel) we show the F_0/R_* -ratios for a bulge 12.6 Gyr SSP and 5 younger components of the disk composite SP, where the flux F_0 is given in Jansky (Jy), the radius R_* in units of the solar radius, and the source is placed at 770 kpc. The brightest bulge events, that can occur, have an un-reddened color of about $(R - I) \approx 0.7$. For the ages above 500 Gyr the stars which can cause the brightest lensing events are either very blue, or have a color of about $(R - I) \approx 0.7$ (i.e. PMS stars present for the ages shown here). The very red luminous stars with $(R - I) > 1$ are ineffective sources for bright lensing events since they are so large, implying a smaller magnification at light curve maximum. The numerous (but fainter) turn-off stars of an 12.6 Gyr old stellar population would need a reddening of $E(R - I) \approx 0.45 \text{ mag}$ to show the measured color of $(R - I) = 0.83 \text{ mag}$. Because this translates into an extinction of $A_R \approx E(R - I)/(1 - (\mathcal{A}_I/\mathcal{A}_V)/(\mathcal{A}_R/\mathcal{A}_V)) = 0.45/(1 - 0.482/0.748) = 1.27 \text{ mag}$ these stars can only produce $(R - I) = 0.83$ events which are 13 times fainter than the brightest bulge stars.

The position of GL1 (3'6" south, 2'40" west of the M31 center) supports the assumption that the source star belongs to the bulge population. Using the assumed extinction for the bulge of $\mathcal{A}_R = 0.36 \text{ mag}$ the intrinsic color of GL1 changes to $(R - I)_0 = 0.70$, which is also the source color for the brightest bulge events (see the peak of the flux-to-radius relation for a 12.6 Gyr old bulge star in Fig. 6b). Such a bulge star has an un-extincted absolute brightness of $\mathcal{M}_R = -0.91 \text{ mag}$ and a radius of $R_* = 30R_{\odot}$. This is in good agreement to the (extinction corrected) R-band brightness of -1.00 mag obtained from the light curve fit (see Table 1).

In Fig. 6c (right panel) we show the minimum lens-source distances ($D_{\text{os}} - D_{\text{ol}}$) as a function of brightness, radius and mass $F_0/(R_*/R_{\odot}) \times \sqrt{M/M_{\odot}}$ using the measured flux excess of WeCAPP-GL1 $\Delta F_{\text{meas}} = 10 \times 10.07^{-5} \text{ Jy}$. For bulge stars the largest $F_0 10^{-0.4A}/(R_*/R_{\odot})$ values are of order $4 \times 10^{-8} \text{ Jy}$ (middle panel, red curve). Now using this with the flux excess of GL1 combined with a bulge extinction of $A_R = 0.36 \text{ mag}$, a $1M_{\odot}$ -lens needs a minimum source distance of about 8.1 kpc (green line in the right panel of Fig. 6), a separation where the product of source and lens densities becomes small (Fig. 6a).

In Fig. 7 we combined the Figs. 6a and 6c for the LOS of WeCAPP-GL1 and show the minimum source-lens distances

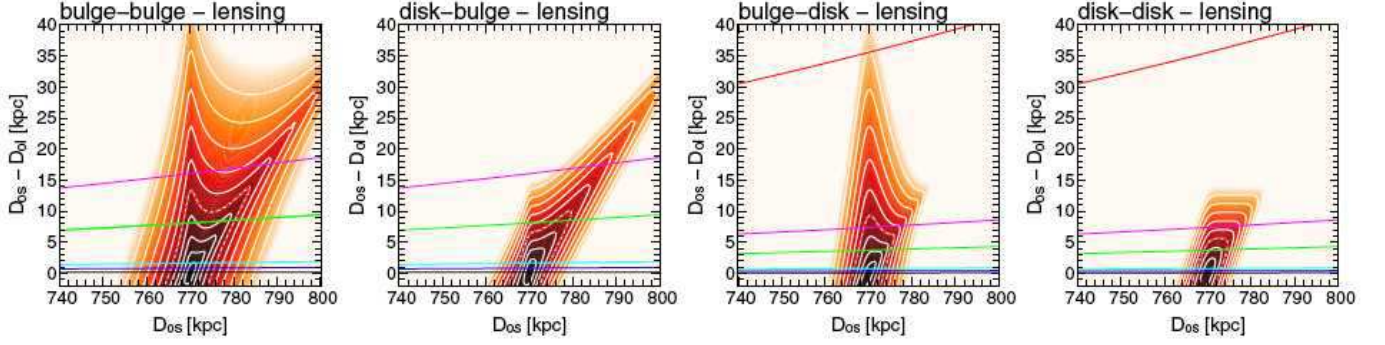


FIG. 7.— Minimum lens-source distance for all self lensing configurations for the WeCAPP-GL1 event, using the intrinsic color of WeCAPP-GL1 of $(R - I)_0 = 0.70$ for bulge sources and $(R - I)_0 = 0.59$ for disk sources and Eq. (4). The red, magenta, green, cyan, blue, black lines represent lenses with masses $0.1M_\odot, 0.5M_\odot, 1M_\odot, 5M_\odot, 10M_\odot$, and $50M_\odot$, respectively. The contours show the product of the density of all source and lens stars (irrespective of color) as a function of the LOS distance to GL1 and the lens-source distance, $\rho_{\text{source}}(\theta_{\text{GL1}}, D_{\text{os}}) \times \rho_{\text{lens}}(\theta_{\text{GL1}}, D_{\text{ol}})$. Contour levels are separated by factors of 10, the dashed contours mark a density of $\rho^2 = 10^{-4}$ (ρ in units of solar masses per cubic parsec).

as a function of the source distance for different self-lensing masses ($M_0 = 0.1, 0.5, 1, 5, 10, 50 M_\odot$). The two peaks in the density contours arise from the maxima in the source density and lens density, respectively. It can easily be seen that lowering D_{os} would slightly decrease the needed lens-source separations, but at the same time the source density decreases rapidly.

For bulge sources at 770 kpc in Fig. 7 a,b the minimum source-lens separation is $D_{\text{os}} - D_{\text{ol}} = 74$ kpc for a low mass lens with $M_0 = 0.1M_\odot$, 16 kpc for a $0.5M_\odot$ lens, and 8.1 kpc for $1M_\odot$. For masses lower than $0.5M_\odot$ the large lens-source distance required to create the observed lensing event, implies a very small event probability, because for large lens-source LOS distances either the source or the lens density is small. So, from just using the brightness of the event, lensing of bulge stars $\leq 0.5M_\odot$ is very unlikely. For a bulge source more reasonable lenses for self lensing are high mass bulge remnants ($D_{\text{os}} - D_{\text{ol}} = 0.16$ kpc for $50M_\odot$) or very rare, young, high mass disk stars (0.82 kpc for $10M_\odot$, 1.6 kpc for $5M_\odot$).

Despite the lower disk density at the position of GL1 disk sources lensed by bulge remnants or high mass disk stars seem more plausible (see the two right panels of Figs. 7c and 7d). We used a reasonable disk extinction of $A_R = 0.68$ mag with the source color and brightness derived from the light curve fit. These values are only consistent with a population older than ≥ 0.5 Gyr (see blue marker in Fig. 2a). Therefore for these disk sources the maximum F_0/R_* -ratio (at $(R - I) = 0.59$ mag) is obtained by stars with $M_R = -1.83$ mag and $R_* = 35.1R_\odot$.

For a disk source at 770 kpc a lens with $1M_\odot$ has to be separated by 3.7 kpc; for a lens with $M_0 = 5M_\odot$ this separation becomes 0.75 kpc. The distances are smaller, since the disk sources are intrinsically brighter, and thus a lower magnification is needed for the event, and therefore, lenses can be closer to the source.

Of course, the event rate contribution is not just proportional to the mass density product of all lenses and all sources (the product of that is displayed as contours in Fig. 7) but depends on the number density of those sources and lenses only that can produce the observed event. There, the (M/L) , and other stellar population properties (fluxes of post-main sequence stars, fraction of stars in a certain color interval) enter.

However our qualitative result, that WeCAPP GL1 lenses below $0.5M_\odot$ for bulge sources and below $0.1M_\odot$ for disk sources are very unlikely, is consistent to the quantitative result in Fig. 8.

5. QUANTITATIVE WECAPP-GL1 ANALYSIS INCLUDING FINITE STELLAR SIZES

In §3 we treated stars as point sources, like Riffeser *et al.* (2003). We now abandon the point source approximation and use for each star the radius based on the isochrones from Girardi *et al.* (2002). We evaluate Eq. C11, using the stellar source size distributions, and show the results in Fig. 8.

Figure 8 shows the halo lensing and self lensing event rates (per flux excess and FWHM-time of the event and per year and square arc minute) at the location of WeCAPP-GL1 using its brightness, time-scale and color and the extended stellar sizes. Comparison to Fig. 4 shows, that self lensing becomes dramatically suppressed; the vertical scale changed by one order of magnitude relative to Fig. 4. The halo-bulge lensing rate decreases by a factor of 6 relative to the point-source formalism. The self lensing rate however decreases much more dramatically using the finite source description. Relative to the most likely M31 halo-bulge lensing, self lensing (bulge-bulge, disk-bulge, disk-disk and bulge-disk) is about 2 orders of magnitude less likely, e.g. lensing of a bulge star by a $0.8M_\odot$ MACHO in M31 (black points) is 119 times more likely as bulge-bulge (red curve) or bulge-disk (green curve) self lensing. The total halo-lensing contribution (summing over M31 and MW halo-bulge and halo-disk lensing) is 63 times more likely than all self lensing contributions assuming a 100% MACHO halo. In addition, for each lensing configuration, the probability for small lens masses is reduced. This can be explained as follows: The large magnification needed for bright events can be obtained in the point source approximation either by large Einstein radii (efficient source-lens geometry or large lens masses) or events with small impact parameter. For point sources, the magnification can formally become infinitely large if the source passes the LOS to the lens. For extended sources the magnification saturates once the source comes closer to the lens LOS than its projected source radius. The source radius projected onto the lens plane is the larger,

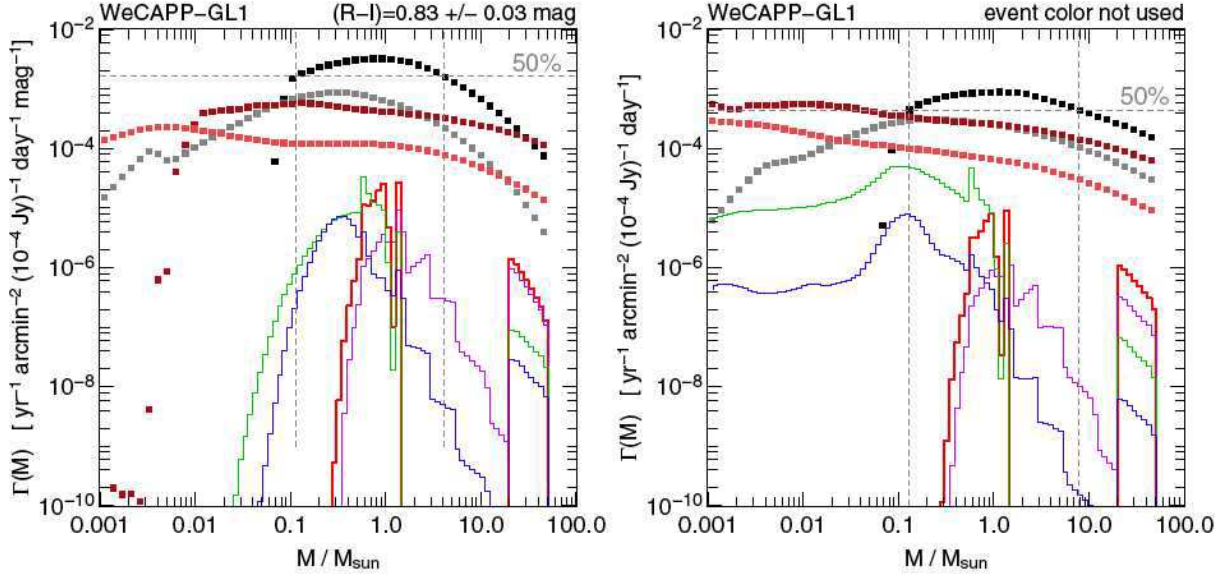


FIG. 8.— Event rate $\Gamma(M)$ (per area, per event brightness ΔF , per event time scale t_{FWHM} , per color $(R-I)$) for WeCAPP-GL1 using the evolved MF including remnants. The lens mass probability was determined allowing for **finite stellar sizes**, using the measured $t_{\text{FWHM}}^{\text{meas}}$, Δ_F^{meas} and C^{meas} of the event $[(R-I)_0 = 0.59$ for disk sources, $(R-I)_0 = 0.70$ for bulge sources, with a Gaussian error of 0.1], assuming a mean M31 extinction of 0.19 and 0.51 for bulge and disk stars, and a MW extinction of 0.17 (in the R-band). The red, green, blue and purple curves show the lens mass distribution function for bulge-bulge, bulge-disk (bulge lens and disk source), disk-bulge and disk-disk lensing. The information about halo lensing (M31-halo-bulge and M31-halo-disk data points are in black and grey, and MW-halo-bulge and MW-halo-disk in brown and orange) is displayed as points and not by a curve: we assume a mono-mass-spectrum for the halos, and each point represents a halo which is made of a given MACHO-mass to 100%.

the closer the lens-source pair, and therefore self lensing events are most strongly suppressed in magnification and thus in flux excess at the light curve maximum. The only way to obtain bright events with finite source sizes is to have spatially well separated source and lens stars (increasing the Einstein radii and decreasing the projected stellar sizes) or to have large lens masses (increase of Einstein radii). Therefore $0.1M_\odot$ (for M31-halo-bulge lensing) and $0.01M_\odot$ (M31-halo-disk lensing) MACHOs have too small Einstein radii to achieve the required large magnification once finite source sizes are taken into account. The suppression sets in for smaller lens masses in the M31-halo-disk lensing case, because disk stars are brighter than bulge stars.

To illustrate the differences between point source and extended source sizes approximation in more detail, we evaluate Eq. (C8) and separate the events into those which do not show any finite source signatures in their light curves (no fss) and those which show finite source signatures (with fss) and display the corresponding results in Figs. 9 and 10.² To understand the differences to Fig. 5 it is useful to recall the relations for event time scale t_{FWHM} and magnification of events at light curve maximum A_0 in the high magnification approximation [for carrying out the integrals we used the exact relations described in Riffeser *et al.* (2006)]:

$$\begin{cases} t_{\text{FWHM}}^{\text{no fss}}(b) \equiv t_{\text{FWHM}}(b) \propto t_E u_0 = t_E \frac{b}{R_E} = v_t^{-1} b & , \quad b \geq b^* \\ t_{\text{FWHM}}^{\text{with fss}}(b) \equiv t_{\text{FWHM}}^*(b) \approx t_{\text{FWHM}}(b) \frac{1}{\sqrt{3}} \sqrt{(2b^*/b)^2 - 1} > t_{\text{FWHM}}(b) & , \quad b < b^* \end{cases} \quad (5)$$

$$\begin{cases} A_0^{\text{no fss}}(b) \equiv A_0(b) \approx R_E/b & , \quad b \geq b^* \\ A_0^{\text{with fss}}(b) \equiv A_0(b^*) \approx R_E/b^* & , \quad b < b^* \end{cases} \quad (6)$$

with $b^* \approx R_* D_{\text{ol}}/(2D_{\text{os}})$. In the point source approximation, source lens configurations with small transverse velocity and small impact parameter can contribute to the event rate at given t_{FWHM} ; in the finite source treatment, transverse velocities have to be larger than a limit $v_t^* \propto b^*/t_{\text{FWHM}}$ to make events without finite source signatures (no fss); in the other case, $v_t < v_t^*$, light curves will show finite source signatures (with fss) (i.e. show a saturated magnification, and an increased event time scale). Therefore, Fig. 10 can be constructed out of Fig. 5, by moving the event rate contributions due to events with $v_t < v_t^*$ to events with finite source signatures, after accounting for their increased time scale, and their decreased brightness. By comparing the panels in the last row in figures Figs. 5 and 9 one can see that finite source effects are almost unimportant for Milky Way MACHO-events with lens masses between $0.2M_\odot$ and $100M_\odot$: for both MACHO masses, the event rate and the characteristics of the events with time scales larger than 1 d (which are observable with present experiments) are nearly the same in the point source approximation and in the extended source size treatment. The remaining panels in Fig. 9 show, that finite source effects are less important for

² To convert to the same units as in Fig. 8 use Eq. C8. E.g. in Figs. 9 and 10 the WeCAPP-GL1 measurements cross the contour level of halo_{M31}($M=0.2M_\odot$)-bulge lensing at -2.30 and -1.86, respectively. This converts to $\Gamma/[\text{yr}^{-1} \text{arcmin}^{-2} \text{mag}^{-1}] = (10^{-2.30} + 10^{-1.86})/(0.4 \ln(10)^2 \cdot 1.83 \text{ day} \cdot 10.07 \times 10^{-5} \text{ Jy}) \times 10^{-4} = 4.8 \times 10^{-3} (10^{-4} \text{ Jy})^{-1} \text{ day}^{-1}$.

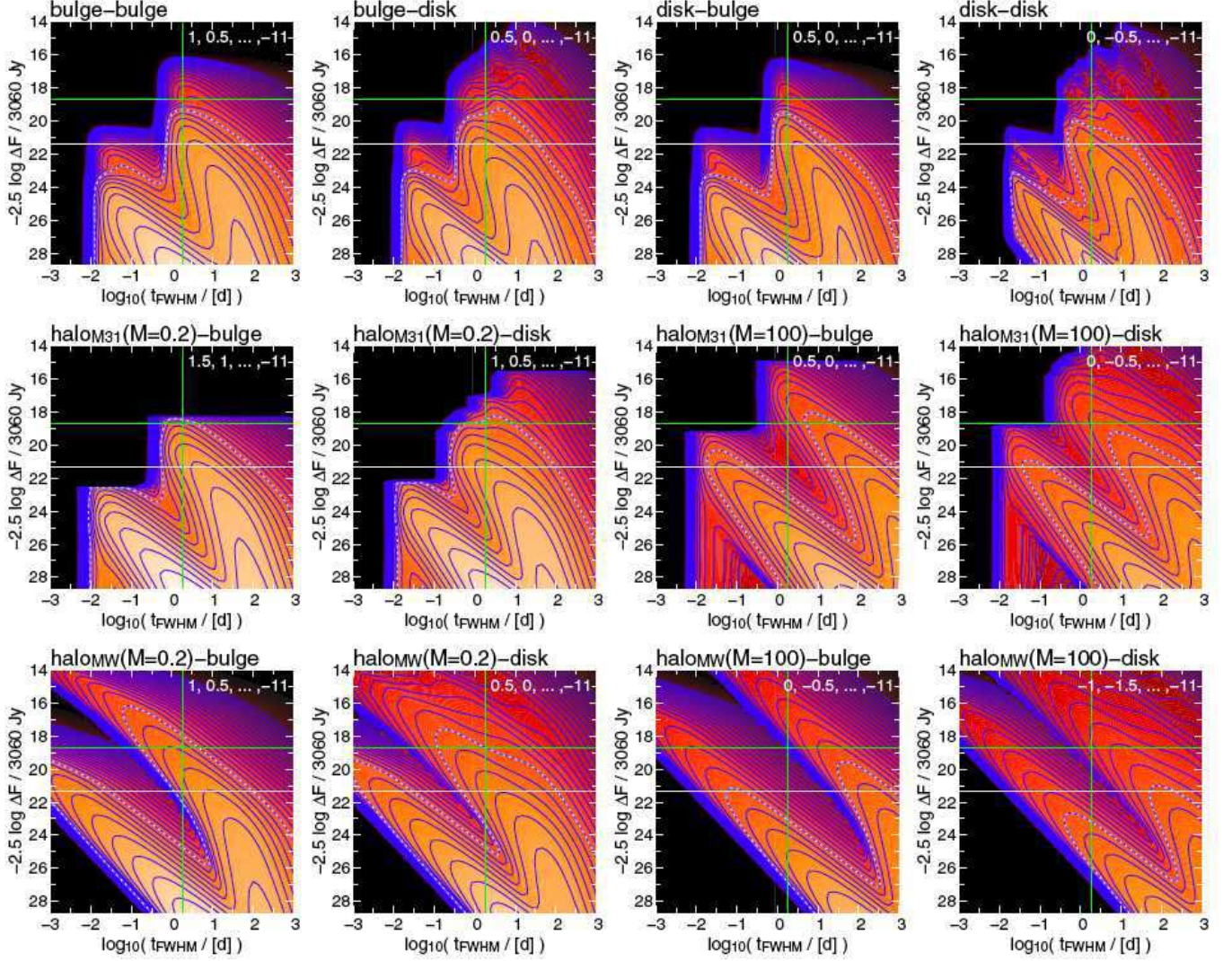


FIG. 9.— Flux excess and time scale distribution of events **with** WeCAPP-GL1 color $((R - I)_0 = 0.59$ for disk sources, $(R - I)_0 = 0.70$ for bulge sources, without using its error) and its location. We make use of **finite stellar sizes** in Eq. C8 but display only events which do **not show any finite source signatures (no fss)** in their light curves (left part of brackets in rhs part of Eq. 2). The two further observables of WeCAPP-GL1 (flux excess and event time scale obtained from a point source lensing light curve fit) are marked in *green*. The estimate for the WeCAPP 6σ detection limit (see Riffeser *et al.* (2006), Table 1) at the position of GL1 is shown as *white line*. The contours differ by $10^{-0.5}$, and the dashed contour is that of 10^{-3} events per year, per square arc minute at location of WeCAPP-GL1, per color (in magnitudes), per logarithmic timescale (time scale in days) and per flux-excess (converted to magnitudes) (see footnotes 3 and 2).

heavy M31-MACHOs, and are relevant for low mass M31-MACHOs, like $0.2M_\odot$ (second row sub panels), and that they are extremely important for the correct interpretation of the self lensing contribution (first row sub panels): an event like WeCAPP-GL1 can hardly be caused by MACHOs with masses much smaller than $0.2M_\odot$, otherwise the flux-excess cutoff would be lower than the event brightness, and WeCAPP-GL1 is unlikely to be caused by self lensing. Among all self lensing scenarios (Fig. 9, first row) the brightness of WeCAPP-GL1 is most easily to achieve by bulge lenses (Fig. 9, *first two panels of the first row*), because in that case source and lens stars are relatively separated (more than for disk lenses).

In Table 3 we have evaluated the number of events we expect to find with time scales between 1 and 3 days in the entire $17.2' \times 17.2'$ field monitored by WeCAPP (assuming 100% detection efficiency). Short self lensing events with a peak magnitude³ larger than 19.0 mag (as lower limit for WeCAPP-GL1, see §4) in the should take place only every 49 years. For reasonable halo mass fraction of 20% consisting of $1M_\odot$ -MACHOs every 10 yrs (short) events above a 19.0 mag threshold could be observed. These values decrease very rapidly lowering the threshold to the most likely peak brightness for GL1 of 18.7 mag: The mean time between events for selflensing is 99 yr whereas for halo lensing 18 yrs. While for the short, fainter events (≤ 21.1 mag) self-lensing would dominate by a factor of 3. Note that these values represent the theoretical event rates in the WeCAPP field without detection bias. In other words only if a survey is complete to a certain threshold it should be possible to measure these numbers of events. For real

³ We define the function $\text{mag}_R(x)$ to replace the transformation from fluxes to magnitudes $\text{mag}_R(x) \equiv -2.5 \log_{10}(x/F_{\text{Vega},R})$ with $F_{\text{Vega},R} = 3060 \text{ Jy}$. The inverse is defined as $\text{flux}_R(x) \equiv F_{\text{Vega},R} 10^{-0.4x}$.

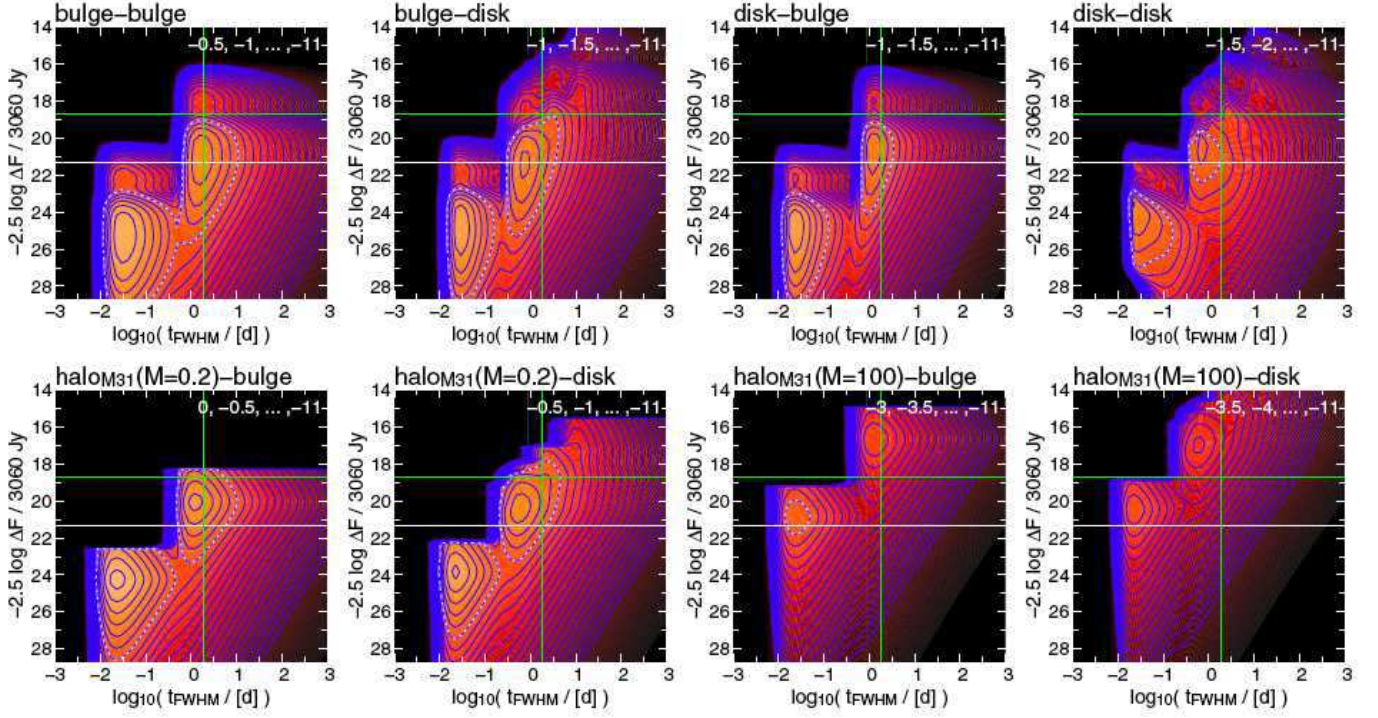


FIG. 10.— Flux excess and time scale distribution of events **with** WeCAPP-GL1 color $[(R - I)_0 = 0.59]$ for disk sources, $(R - I)_0 = 0.70$ for bulge sources, without using its error] and its location. We account for **finite stellar sizes** in Eq. C8 but add only events (right part of brackets in rhs part of Eq. 2) which do **show finite source signatures (with fss)**. The two further observables of WeCAPP-GL1 (flux excess and event time scale obtained from a point source lensing light curve fit) are marked in *green*. The estimate for the WeCAPP 6σ detection limit (see Riffeser *et al.* (2006), Table 1) at the position of GL1 is shown as *white line*. The contours differ by $10^{-0.5}$, and the dashed contour is that of 10^{-3} events per year, per square arc minute at location of WeCAPP-GL1, per color (in magnitudes), per logarithmic timescale (time scale in days) and per flux-excess (converted to magnitudes) (see footnotes 3 and 2).

type	ΔF_R [10^{-5} Jy]	$\text{mag}_R(\Delta F_R)$ [mag]	event rate [ev/yr]	mean time between events [yr]
self lensing	≥ 10	≤ 18.7	0.0101	99.2
"	≥ 8	≤ 19.0	0.0204	49.0
"	≥ 0.9	≤ 21.3	6.47	0.155
halo lensing with 20% $1M_\odot$	≥ 10	≤ 18.7	0.0541	18.5
"	≥ 8	≤ 19.0	0.0969	10.3
"	≥ 0.9	≤ 21.3	2.21	0.45

TABLE 3

EXPECTED RATES FOR SHORT TIME SCALE (FWHM-TIMESCALES BETWEEN 1 AND 3 DAYS) LENSING EVENTS IN THE ENTIRE $17.2' \times 17.2'$ WECAAPP, ASSUMING 100% DETECTION EFFICIENCY.

microlensing surveys the detection efficiency for bright events will be much higher than for faint events, and therefore the ratio of bright vs. short events would be different. If we assume to have the same detection efficiency for halo and selfensing (which in principle can differ according to their intrinsic distribution) the difference between halo-lensing and self lensing favors the assumption that WeCAPP-GL1 (*green line*) was caused by a halo lens.

To summarize, an event as bright as WeCAPP-GL1 is extremely unlikely to be a self lensing event. The most likely self lensing scenario is bulge-disk self lensing. MACHO-lenses above 0.2 solar masses are expected to cause the bright events much easier.

6. INTERPRETING WECAAPP-GL1: IMPACT OF EXTINCTION

Riffeser *et al.* (2006), which assumes an on average M31-extinction for all disk stars in the WeCAPP field of 0.51 mag and for all bulge stars of 0.19 mag in the R-band, independent of the angular position of the event, and independent of the LOS distance to the source. The MW-extinction is set to 0.17 mag (R-band). The result for this M31 standard-dust model has been described in Fig. 8 already.

To see to which extent dust can change the interpretation of lensing events, we set the M31-extinction (not the MW-extinction) along the LOS to WeCAPP-GL1 to zero. We do not assume that the mean M31-extinction of bulge or disk stars goes to zero as well⁴, but that by accident just this one sight line to the source is not extinguished by

⁴ This would imply a decrease of the disk and bulge number density and thus of the event rates for disk source stars by 37% and for bulge source stars by 16% and thus would decrease the lensing rate of disk sources relative to bulge sources

M31-dust at all; the extinction then equals that of the MW of about 0.17 mag. The results are shown in the left-most column of panels in Fig. 11. With no M31-dust along the LOS to WeCAPP-GL1 the event would become intrinsically fainter (relative to the extinction case and giving the observed fluxes) by 0.19 mag and 0.5 mag in the R-band for bulge and disk sources. This reduces the necessary magnification and makes self lensing more likely. At the same time the lensed sources are expected to be intrinsically redder, which changes the stellar types of stars and thus its absolute brightness (*lower panels*). One can derive the increase of the event rates for an event like WeCAPP-GL1 also by shifting the contours in Figs. 9 and 10 by 0.19 mag and 0.51 mag along the ΔF -direction for lensing of bulge sources and disk sources respectively. The ratio for the event rates of all self-lensing to all halo-lensing configurations is still of the order of 1:100 for full MACHO halos and MACHO masses in the range of 0.1 to 1 solar masses. So even in the implausible case of no M31-dust along the LOS to the source of WeCAPP-GL1, a 1% MACHO fraction of the M31 and MW halos already provides the same lensing rates as self lensing does.

As alternative values for the total (MW+M31) line of sight extinctions we also use values of 0.7 mag and 1.05 mag (“strong extinction”) and show the results in the third and fourth columns of Fig. 11. In this case lensing rates are suppressed and the most likely lens masses are shifted to higher masses. This can be understood since now only higher mass lenses are able to provide the high flux excess found for WeCAPP-GL1.

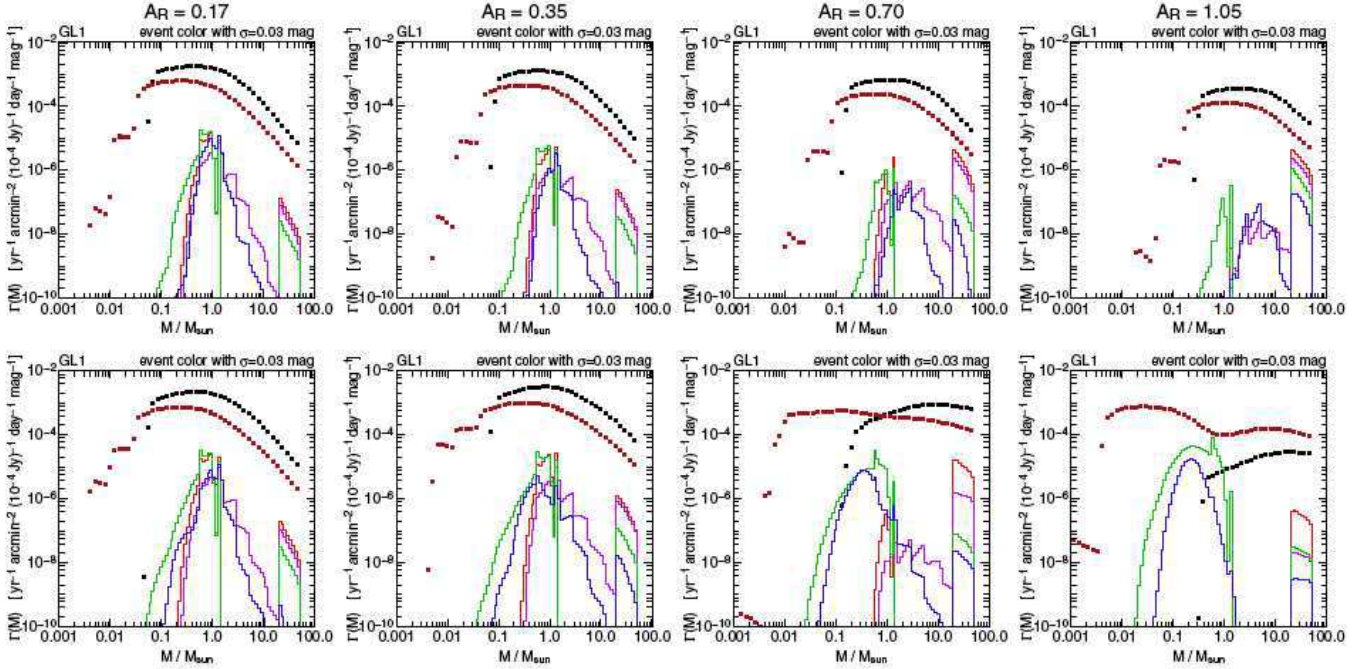


FIG. 11.— Event rate $\Gamma(M)$ (per area, per event brightness ΔF , per event time scale t_{FWHM} , per color $(R-I)$) for WeCAPP-GL1. *upper panels*: without changing the color by the assumed extinction [$(R-I)_0 = 0.59$ for disk sources, $(R-I)_0 = 0.70$ for bulge sources, with a Gaussian error of 0.03], *lower panels*: taking into account the color shift due to the assumed extinction. The red, green, blue and purple curves show the event rate for bulge-bulge, bulge-disk (bulge lens and disk source), disk-bulge and disk-disk lensing. The information about halo lensing (M31-halo-bulge and M31-halo-disk data points are in black and grey, and MW-halo-bulge and MW-halo-disk in brown and orange) is displayed as points and not by a curve: we assume a mono-mass-spectrum for the halos, and each point represents a halo which is made of a given MACHO-mass to 100%. The results have been obtained with an average dust extinction of total bulge and disk population of $\mathcal{A}_R = 0.36$ mag and $\mathcal{A}_R = 0.68$ mag. These values are expressed in the two middle panels as 0.35 and 0.7. The results for the minimum line of sight extinction of 0.17 (set by the MW) and for a high extinction of 1.05 are shown to the left and right of the same row. The 4 panels in the first row show results analogous to the 2nd row, with the difference, that the de-reddening of the source star has been neglected: this simplification would have a minor impact on the interpretation for the stellar populations assumed here.

In the second row of Fig. 11 we show how the extinction influences the color of the event and therefore the type of source stars which were most likely lensed. Whereas in the upper panels the event rates are shown, if one accounts for the dimming but not for the reddening by dust, in the lower panels we take into account the reddening with the assumed extinction. The effect is lowest for low extinction; for high extinctions the predicted masses are strongly changed. The assumed shifts in color $(R-I)$ for event extinctions of 0.17, 0.35, 0.70, 1.05 mag are -0.06, -0.12, -0.25, -0.37, respectively, which means that the **intrinsic** colors of GL1 are 0.77, 0.71, 0.58, 0.46. Comparing these colors with the CMD in Fig. 2, shows that the intrinsic brightness can drastically change for slight color differences: for the 12.6 Gyr component from -1.0 to +3.7 mag, for the 2.5 Gyr disk component from -1.8 to +2.3, whereas the 20 Myr disk component slightly brightens from -6.2 to -6.9 mag. This can explain the extreme differences in the lens mass distributions and underlines the importance of accurate color measurements and precise extinction estimates. Although the color plays an important role in the correct mass interpretation, the ratio between halo- and self-lensing is almost independent of the assumed extinction. For all extinction assumptions WeCAPP-GL1 is more likely caused

by a halo lens than by a stellar lens. Only for the de-reddened, high extinction case (*last panel, 2nd row*) the halo to self-lensing ratio approaches a factor of 10.

7. THE IMPACT OF A METAL POORER DISK

The maximum flux excess ΔF of an event depends on the flux and radius of the source star. Therefore, the question arises, how sensitive the interpretation, that WeCAPP-GL1 can hardly be achieved by self lensing, depends on the assumed metallicity of the stellar population. The luminosity and sizes of post-main-sequence stars change slightly, if the metallicity of the composite stellar population is altered.

We therefore have modeled a metal poorer disk (Williams 2002) by changing the metallicities to $Z = 0.008$ (see Girardi's `isoc_z008.dat`). The change of metallicity has several competing effects:

- i) a metal poorer population is brighter
- ii) for a metal poorer population, smaller MACHOs masses are allowed, since brighter stars need smaller magnification, which can be produced also by smaller masses without finite-source-size saturation of the magnification.
- iii) the lens properties are nearly not affected by the luminosity evolution, since reducing the metallicity mostly changes the properties for the lensed stars (sources), and mass evolution takes place only for very few stars.
- iv) a stellar population with lower metallicity (changed from solar by a factor of 2) contains PMS star brighter by a factor of roughly 2 (≈ 0.75 mag). Their radii ($R_* \propto \sqrt{F_0}$) are larger by a factor of roughly $\sqrt{2} = 1.4$. Since (see Eq. (3)) $\Delta F_{\max} \propto F_0/R_* \propto \sqrt{F_0} \propto R_*$ for events with the same color, one expects the flux excess of the brightest events to increase by a factor of 1.4, or 0.38 mag if the stars become metal poorer. This would make the contours in Figs. 9 and 10 to shift by 0.38 mag in vertical direction and push the flux-excess limit due to finite source effects by the same amount.
- v) However, if stars are brighter, fewer of them are needed to account for the total observed light, which reduces the overall lensing rate, e.g. the (M/L) of the disk population drops from 1.2 to 1.0 in the R-band if the metallicity of the population is changed from solar to 0.008.

All these points explain the relative small differences in the event rates by changing the metallicity of stellar population. However the lower part of mass probability distribution for a measured event can slightly shift to lower masses, as the lower amplifications can be produced by lower masses.

8. OUTLOOK: STATISTICAL INTERPRETATION - HALO VS. SELF LENSING FROM BRIGHTNESS DISTRIBUTIONS OF EVENTS

We now show that the brightness and time scale distribution of events can be used to discriminate halo and self-lensing.

Figure 12 (*left panels*) compares the event rates as a function of event brightness for self lensing and halo lensing events within rings around the M31 center. These rings have a thickness of 1 arcmin and outer radii between 1 arcmin and 12 arcmin (blue/red for self lensing, green/black for halo lensing). The event rates were calculated ignoring detection efficiency factors, assuming a 12.6 Gyr bulge and a composite disk population, and the mean extinctions for the bulge and the disk sources. We consider only events longer than 1 day (t_{FWHM}). For self lensing, the event rate drops steeper with event brightness within central rings than within outer rings. This is caused because in the inner rings self lensing of bright events is suppressed by the closer LOS distances of source-lens pairs. For the outer rings the mean distances between disk-bulge pairs are larger and the lensing rate is increased. For halo lensing there is no such effect. The brightness cut-off of the event-rate–event-brightness relation is determined mostly by stellar population properties (self lensing) and by the MACHO mass (halo lensing), as can be seen by comparing the left panels in Fig. 12 which were obtained for $0.1M_\odot$, $1.0M_\odot$, and $10M_\odot$ MACHOs from top to bottom. This demonstrates that the brightness distribution of bright events could itself discriminate halo and self lensing if a sufficient large number of events is available. The two lines represent the WeCAPP-GL1 flux excess (fit and highest data point).

The distribution of event time scales (only events brighter than 10^{-5} Jy in R are considered) is fairly similar for self lensing and MACHO events (in slope) if the MACHO mass is $0.1M_\odot$ (this can also be seen from Fig. 9 which shows for the location of GL1 that the event characteristics [flux excess and time scale] are most similar for self lensing and halo lensing if the halo population has a mass of $0.2M_\odot$). However, if MACHO masses are larger, events will have longer timescales than predicted from self lensing (see Fig. 12, right panels).

The right panels in the 2nd and 3rd row of Fig. 12 show the time-scale distribution for $1M_\odot$ and $10M_\odot$ MACHOs, respectively. Because of the clear difference between selflensing and halolensing the time scale-distribution is a good discriminator if the MACHO mass is larger than $1.0M_\odot$.

The sharp cut-off in the brightness distribution of halo-lensing events is caused by the fact that the MACHO mass function used is a *delta*-function. Since the different lensing masses produce a brightness distribution which has quite a different gradient with respect to selflensing, it is conceivable that there exists a specific halo-mass function where the brightness distributions look similar to self-lensing. Therefore, one probably can find a halo mass function that can mimic self lensing as long as only the brightness distribution of events is considered. If one however combines the brightness distribution with the distribution of the time scales and locations of the events, the halo-self-lensing degeneracy can be broken.

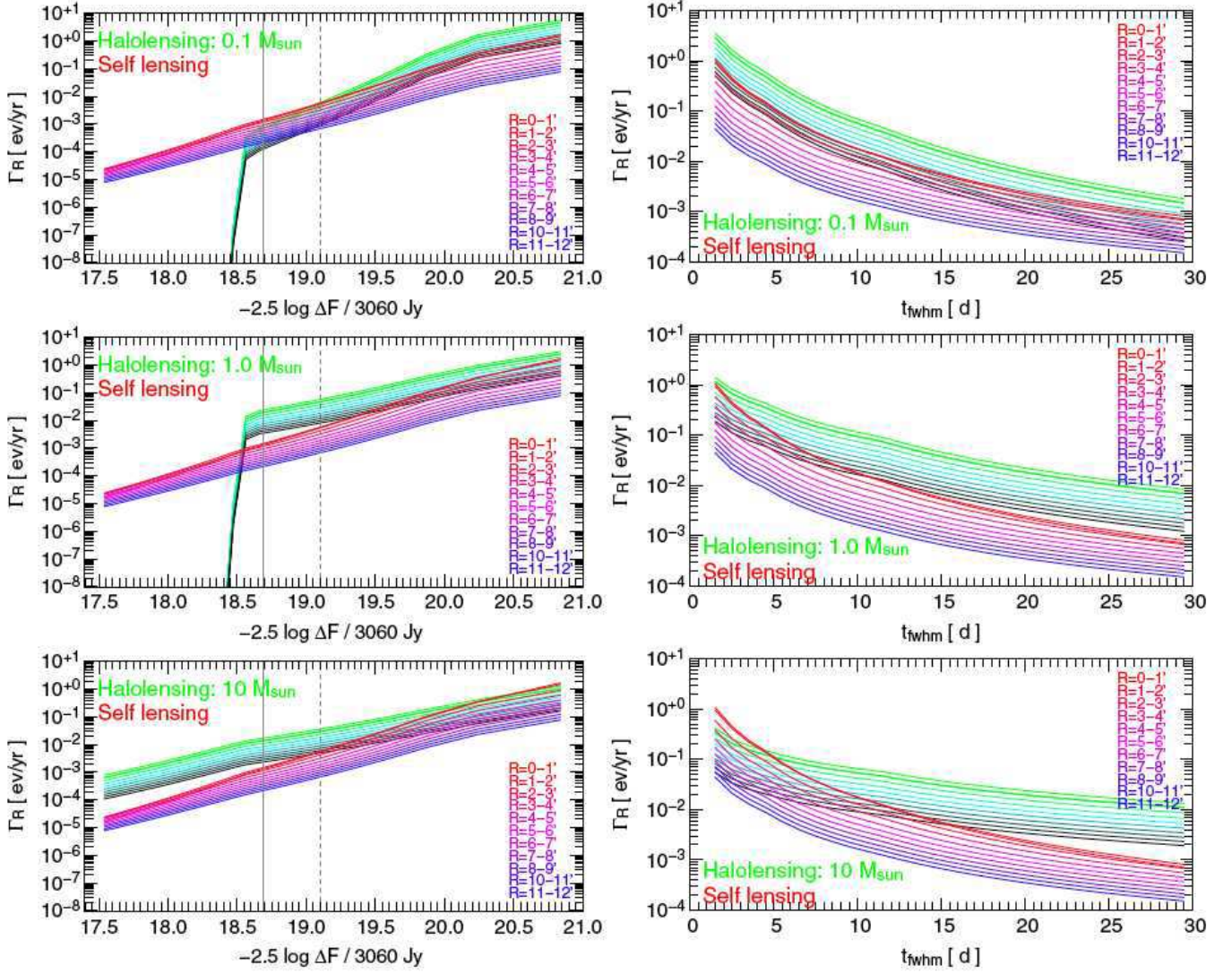


FIG. 12.— *Left panels:* Brightness distribution of events (with $t_{\text{fwhm}} > 1\text{d}$) within rings of 1 arcmin around the M31 center. Outer radii are chosen between 1 arcmin (red for self lensing, black for M31 halo lensing) and 12 arcmin (blue for self lensing, green for halo lensing). The two vertical lines (grey) represent the GL1 flux excess (fit and highest data point). *Right panels:* Time scale distribution of events (brighter than $\Delta F > 10^{-5} \text{ Jy}$ corresponding to an excess magnitude of 21.2) within rings of 1 arcmin around the M31 center. Outer radii are chosen between 1 arcmin (red for self lensing, black for M31 halo lensing) and 12 arcmin (blue for self lensing, green for halo lensing).

9. DISCUSSION AND CONCLUSION

We showed that accounting for extended sources can dramatically change the lensing and self lensing rates for events as bright as WeCAPP-GL1. The reason is that magnification saturates, and that the maximal brightness of an event for a given source size and source flux depends only on the source and lens distances and lens mass (not on the impact parameter): Very bright events thus require a minimum source lens distance, which makes halo lensing more likely relative to self lensing. For WeCAPP-GL1 the inclusion of the finite stellar sizes makes the ratio of self lensing to halo lensing by about a factor of 8 less likely compared to the point source approximation. This result was obtained based on simple stellar population models of the bulge and disk and on a simple description of the dust extinction and is almost independent of MACHO mass as long as that is in a range of $0.1 - 3.5 M_\odot$.

Likewise if one uses position, FWHM time scale, flux excess and color of WeCAPP-GL1, self-lensing is even 13 times less likely than lensing by a MACHO, if 1 solar mass MACHOs contribute only 20% to the total halo mass in this mass range.

Assuming a 100% detection efficiency we expect a self lensing event with with FWHM time-scales between 1 and 3 days and a peak flux excess brighter than 19.0 mag in the *entire* WeCAPP survey field only once every 49 yrs (99 yrs for $\text{mag}_R(\Delta F) < 18.7 \text{ mag}$). On the other hand if 20% of the halos of M31 and the MW are made of 1.0 solar mass MACHOs then an event like WeCAPP-GL1 would occur every 10 years (every 18 yrs for a 18.7 mag threshold).

This implies that a small fraction of baryonic MACHOs like (brown dwarfs, neutron stars, stellar black holes, cool white dwarfs) in the M31 halo is sufficient to make WeCAPP-GL1 more likely to be a halo-lens event.

We have also shown that different values for the extinction of the WeCAPP-GL1 event do only slightly change the halo-lensing – self lensing ratio, but more strongly change the most likely lensing masses. This is because the major impact of the extinction is that of a bluer intrinsic source color and therefore implies a change of stellar source size and brightness.

We emphasize that any interpretation for high difference flux events and their predicted rates has to account for finite-source effects. Further published examples are Ansari *et al.* (1999); Auriere *et al.* (2001); Paulin-Henriksson *et al.* (2003). Therefore the brightness distribution of events in general is a good discriminator between self and halo lensing. The time-scale distribution is a good discriminator if the MACHO mass is larger than $1.0 M_\odot$.

Our model reasonably describes the (M/L) for the stellar population in M31 and we are confident that the mass density and velocity distribution of the stars is fairly well modeled. With these ingredients one cannot obtain an event rate high enough to make a detection of WeCAPP-GL1 likely within our survey interval. Therefore, our analysis supports the existence of a (small baryonic or non-baryonic) MACHO component in the halos of M31 or MW.

In this paper we have ignored detection efficiencies. We were allowed to do so, because, for a single event, the probability *ratio* of halo lensing to self-lensing is independent of detection efficiencies. For WeCAPP-GL1, halo lensing (assuming a 20% MACHO halo) is 5 times more likely than self-lensing. We admit that this factor of 5 is not large enough to conclude that self-lensing is definitely excluded. However, we point out, that 'WeCAPP-GL1'-like self-lensing events are very rare. Put in another way, the fact that this event was observed can be more easily understood, if there is a, e.g., 20% compact dark matter fraction in the halos of M31 and the MW. The analysis of more bright events, and the comparison of the event rates for bright and faint events will give more insight, as well as the use of their time scale distribution. This however requires the knowledge of the detection efficiency (as a function of brightness, timescale, location and color) of the events, and will be subject of a further paper. Our results provide a strong motivation to search for the brightest short time scale events towards M31 in wide field surveys (like Pan-STARRS 1).

APPENDIX

M31-MODEL

Assuming an M31-distance of 770 kpc we converted our light model (described in Riffeser *et al.* (2006)) into mass using the theoretical bulge and disk R-band $(M/L)_R$ of 3.3 and 1.2 derived using their theoretical stellar populations. The colors extracted from these stellar populations are for the bulge $(B - R)_0 = 1.63$ [$(B - R)_{\text{meas}} = 1.91$], $(V - R)_0 = 0.60$ [$(V - R)_{\text{meas}} = 0.72$] and for the disk $(B - R)_0 = 0.81$ [$(B - R)_{\text{meas}} = 1.33$], $(V - R)_0 = 0.37$ [$(V - R)_{\text{meas}} = 0.60$]. The analytical mass density models are

$$\rho_{\text{bulge}}(x, y, z) := 44 \, 100 M_\odot / \text{pc}^3 \times \begin{cases} 10^{-0.4(1.41 a^{1/4})} & a \leq 3.1 \text{ pc} \\ 10^{-0.4(29.7 a^{1/4} - 6.68)} & 3.1 \text{ pc} < a \leq 20 \text{ pc} \\ 10^{-0.4(10.3 a^{1/4} + 0.61)} & a > 20 \text{ pc} \end{cases} \quad (\text{A1})$$

with $a \equiv 0.57z^2 + \sqrt{0.57^2 z^4 + x^2 + y^2 + 1.11z^2}$ in kpc,

$$\rho_{\text{disk}}(x, y, z) = 0.27 M_\odot / \text{pc}^3 \times \exp\left(-\frac{\sqrt{x^2 + y^2}}{h_\sigma}\right) \text{sech}^2\left(\frac{z}{h_z}\right), \quad (\text{A2})$$

with $h_\sigma \equiv 6.4 \text{ kpc}$ and $h_z \equiv 0.3 \text{ kpc}$,

$$\rho_{\text{halo}}(x, y, z) = 0.065 M_\odot / \text{pc}^3 \times \frac{1}{1 + (r/r_c)^2} \quad r \leq 100 \text{ kpc} \quad (\text{A3})$$

with $r \equiv (x^2 + y^2 + z^2)^{1/2}$ and $r_c = 4 \text{ kpc}$.

Integrating over these density profiles gives a total mass for the bulge of $4.44 \times 10^{10} M_\odot$, for the disk of $4.18 \times 10^{10} M_\odot$ and for the halo of $122.7 \times 10^{10} M_\odot$.

We used a bulge and disk inclination of $i = 77^\circ$, a position angle of the disk major axis of $P.A. = 38^\circ$ and $P.A. = 50^\circ$ for the bulge.

For the transversal velocity distribution we assumed

$$p_{v_t}(v_t) = \frac{1}{\sigma_{ls}^2} v_t \exp\left(-\frac{v_t^2 + v_0^2}{2\sigma_{ls}^2}\right) I_0\left(\frac{v_0 v_t}{\sigma_{ls}^2}\right), \quad (\text{A4})$$

with $\sigma_{ls} = [\sigma_l^2 + (\sigma_s D_{ol}/D_{os})^2]^{0.5}$. The velocity dispersions are $\sigma_{bulge} = 100 \text{ km s}^{-1}$, $\sigma_{disk} = 30 \text{ km s}^{-1}$, $\sigma_{halo} = 166 \text{ km s}^{-1}$, $\sigma_{MW-halo} = 156 \text{ km s}^{-1}$. The additional rotations are taken into account as $v_0(D_{os}, D_{ol}, v_{rot,l}, v_{rot,s}, v_{\odot-M31})$, where we used $v_{rot,bulge} = 30 \text{ km s}^{-1}$ and $v_{rot,disk} = 235 \text{ km s}^{-1}$ and an observer's motion of $v_{\odot-M31} = 129 \text{ km s}^{-1}(D_{os} - D_{ol})/D_{os}$.

EVENT RATE

Eq. 2 contains the following analytical functions [we have dropped the variables on the right-hand-side (rhs) mostly; all functions on this side can be expressed as a function of the variables on the left-hand-side (lhs)]

$$\begin{aligned} \Upsilon(\Delta F/F_0 + 1) &= \Upsilon(A_0) = 2\sqrt{u\left(\frac{A_0+1}{2}\right)^2 - u(A_0)^2} = \sqrt{8} \frac{[(A_0+1)^{3/2} - A_0(A_0+3)^{1/2}]^{1/2}}{[(A_0-1)(A_0+1)(A_0+3)]^{1/4}} \\ \Psi(\Delta F/F_0 + 1) &= \left|\frac{du_0}{dA_0}\right| \Upsilon^2(A_0) = 4\sqrt{2} \frac{[A_0 + (A_0^2 - 1)^{1/2}]^{1/2} [(A_0+1)^{3/2} - A_0(A_0+3)^{1/2}]}{(A_0^2 - 1)^{7/4} (A_0+3)^{1/2}} \\ D_{ol}^*(R_*, D_{os}, M, \Delta F, F_0) &= D_{os} \left(1 + \frac{\Delta F(2F_0 + \Delta F)}{C D_{os}}\right)^{-1} \quad \text{with} \quad C := \frac{16 F_0^2 G M}{c^2 R_*^2} \\ u_0^*(R_*, D_{ol}, D_{os}, M) &= \left(2 \left(1 + \left(\frac{R_* D_{ol}}{2 R_E D_{os}}\right)^2\right)^{1/2} - 2\right)^{1/2} \\ &\quad \text{with} \quad R_E := \frac{\sqrt{4 G M}}{c} \sqrt{\frac{D_{ol}(D_{os} - D_{ol})}{D_{os}}} \\ \Omega^*(\Delta F, D_{os}, F_0, M, R_*) &= \left|\frac{dD_{ol}^*(\Delta F)}{d\Delta F}\right| = 2 C D_{os}^2 (F_0 + \Delta F) (C D_{os} + \Delta F(2F_0 + \Delta F))^{-2} \\ \Upsilon^*(u_0, R_*, D_{ol}, D_{os}, M) &= 2\sqrt{\frac{2(A_0^*+1)}{\sqrt{(A_0^*-1)(A_0^*+3)}}} - 2 - u_0^2 \quad \text{with} \quad A_0^* = \sqrt{1 + \left(\frac{2 R_E D_{os}}{R_* D_{ol}}\right)^2} \\ v_t(D_{ol}, D_{os}, M, t_{FWHM}, \Delta F, F_0) &= \frac{R_E(D_{ol}, \dots)}{t_{FWHM}} \Upsilon \\ v_t^*(u_0, D_{ol}, D_{os}, M, t_{FWHM}, R_*) &= \frac{R_E}{t_{FWHM}} \Upsilon^*(u_0, \dots) \end{aligned}$$

and the color-magnitude relations of stars, $p_{cmd}(\mathcal{M}, \mathcal{C})$, the mass function of stars and potential MACHOs, $\xi(M)$, the spatial density of **sources** $n(x, y, D_{os})$ on the line of sight, the mass density of **lenses**, $\rho(x, y, D_{ol})$, and the transversal projected lens-source velocity distribution $p_{v_t}(v_t)$. The mass density of lenses depends on the dynamical model and the number density of sources is constrained by the observed light of the stellar population. If the extinction value of the stellar population changes, or equivalently, the (M/L) of the stellar population is changed, the event rate scales linearly (and not quadratically).

The first term inside the brackets of the rhs of Eq. 2 collects contributions from events that do not show finite source signatures, i.e. events with impact parameters larger than the projected source radius, $u_0 > u_0^* \approx R_* D_{ol} (2 R_E D_{os})$ (see Eqs. 65 and 66 in Riffeser *et al.* (2006)). The second term on the rhs is due to events showing finite source signatures, i.e. events with impact parameters closer than the projected source radius, $u_0 < u_0^*$, we used Eq. 67 in Riffeser *et al.* (2006).

All functions with “*” depend on the radius $R_*(\mathcal{M}, \mathcal{C})$.

LENS MASS PROBABILITY DISTRIBUTION

The event rate differential in Eq. (2) depends on 7 arguments: The first 5 arguments ($x, y, t_{FWHM}, \Delta F, \mathcal{C}$) are observables of lensing events; the brightness of the source stars, \mathcal{M} , is not directly observable in light curves (the color-luminosity distributions of stars can instead be statistically described using observations of resolved stellar populations in M31 or using stellar population models); the sixth argument, the lens mass, M , is the quantity to be statistically constrained (lens mass functions and amplitudes) from observing lensing events. One can integrate Eq. (2) to obtain lower order differentials:

$$\frac{d^6 \Gamma(x, y, t_{FWHM}, \Delta F, \mathcal{C}, M)}{dx dy dt_{FWHM} d\Delta F d\mathcal{C} dM} = \int \frac{d^7 \Gamma(x, y, t_{FWHM}, \Delta F, \mathcal{C}, M, \mathcal{M})}{dx dy dt_{FWHM} d\Delta F d\mathcal{C} dM d\mathcal{M}} d\mathcal{M} \quad (\text{C1})$$

$$\frac{d^5 \Gamma(x, y, t_{FWHM}, \Delta F, \mathcal{C})}{dx dy dt_{FWHM} d\Delta F d\mathcal{C}} = \int \int \frac{d^7 \Gamma(x, y, t_{FWHM}, \Delta F, \mathcal{C}, M, \mathcal{M})}{dx dy dt_{FWHM} d\Delta F d\mathcal{C} dM d\mathcal{M}} d\mathcal{M} dM \quad (\text{C2})$$

$$\frac{d^4\Gamma(x,y,t_{\text{FWHM}},\Delta F)}{dx dy dt_{\text{FWHM}} d\Delta F} = \int \int \int \frac{d^7\Gamma(x,y,t_{\text{FWHM}},\Delta F,\mathcal{C},M,\mathcal{M})}{dx dy dt_{\text{FWHM}} d\Delta F d\mathcal{C} dM d\mathcal{M}} d\mathcal{M} d\mathcal{C} dM \quad (\text{C3})$$

In the following we assume, that one can measure the location of an event without any error. Some of the remaining observables $(t_{\text{FWHM}}, \Delta F, \mathcal{C})$ might have fairly large errors. Let $p(o, o^{\text{meas}})$ be the probability for measuring o^{meas} with o being the true value. We then can estimate the error-weighted values of the differentials in Eqs. C1, C2 and C3 at the location of the observables:

- without color measurement

$$\left\langle \frac{d^4\Gamma(x,y,t_{\text{FWHM}},\Delta F)}{dx dy dt_{\text{FWHM}} d\Delta F} \right\rangle_{x^{\text{meas}}, y^{\text{meas}}} (t_{\text{FWHM}}, \Delta F) := \frac{d^4\Gamma(x^{\text{meas}}, y^{\text{meas}}, t_{\text{FWHM}}, \Delta F)}{dx dy dt_{\text{FWHM}} d\Delta F} \quad (\text{C4})$$

$$\begin{aligned} \left\langle \frac{d^4\Gamma(x,y,t_{\text{FWHM}},\Delta F)}{dx dy dt_{\text{FWHM}} d\Delta F} \right\rangle_{x^{\text{meas}}, y^{\text{meas}}, t_{\text{FWHM}}^{\text{meas}}, \Delta F^{\text{meas}}} &:= \\ \int \int \frac{d^4\Gamma(x^{\text{meas}}, y^{\text{meas}}, t_{\text{FWHM}}, \Delta F)}{dx dy dt_{\text{FWHM}} d\Delta F} p(t_{\text{FWHM}}, t_{\text{FWHM}}^{\text{meas}}) p(\Delta F, \Delta F^{\text{meas}}) dt_{\text{FWHM}} d\Delta F & \end{aligned} \quad (\text{C5})$$

$$\begin{aligned} \left\langle \frac{d^5\Gamma(x,y,t_{\text{FWHM}},\Delta F,M)}{dx dy dt_{\text{FWHM}} d\Delta F dM} \right\rangle_{x^{\text{meas}}, y^{\text{meas}}, t_{\text{FWHM}}^{\text{meas}}, \Delta F^{\text{meas}}} (M) &:= \\ \int \int \int \frac{d^5\Gamma(x^{\text{meas}}, y^{\text{meas}}, t_{\text{FWHM}}, \Delta F, M)}{dx dy dt_{\text{FWHM}} d\Delta F dM} p(t_{\text{FWHM}}, t_{\text{FWHM}}^{\text{meas}}) p(\Delta F, \Delta F^{\text{meas}}) dt_{\text{FWHM}} d\Delta F & \end{aligned} \quad (\text{C6})$$

- with color measurement $\mathcal{C}^{\text{meas}}$

$$\begin{aligned} \frac{d^2\Gamma(t_{\text{FWHM}}, \Delta F)}{dt_{\text{FWHM}} d\Delta F} &:= \\ \left\langle \frac{d^5\Gamma(x,y,t_{\text{FWHM}},\Delta F,\mathcal{C})}{dx dy dt_{\text{FWHM}} d\Delta F d\mathcal{C}} \right\rangle_{x^{\text{meas}}, y^{\text{meas}}, \mathcal{C}^{\text{meas}}} (t_{\text{FWHM}}, \Delta F) &:= \int \frac{d^5\Gamma(x^{\text{meas}}, y^{\text{meas}}, t_{\text{FWHM}}, \Delta F, \mathcal{C})}{dx dy dt_{\text{FWHM}} d\Delta F d\mathcal{C}} p(\mathcal{C}, \mathcal{C}^{\text{meas}}) d\mathcal{C} \end{aligned} \quad (\text{C7})$$

Eq. C7 can be transformed (To transform a distribution $df(x)/dx$ to $dg(u)/du$ with $u(x)$ and its inverse $x(u)$ we used $dg(u)/du = df[x(u)]/dx |dx(u)/du|$, see also footnote 3) into

$$\frac{d^2\tilde{\Gamma}(\vartheta, \delta_m)}{d\vartheta d\delta_m} = 0.4 \ln(10)^2 10^\vartheta \text{flux}_R(\delta_m) \frac{d^2\Gamma(10^\vartheta, \text{flux}_R(\delta_m))}{dt_{\text{FWHM}} d\Delta F} \quad (\text{C8})$$

defining $\vartheta \equiv \log_{10} t_{\text{FWHM}}$ and $\delta_m \equiv \text{mag}_R(\Delta F)$.

$$\begin{aligned} \left\langle \frac{d^5\Gamma(x,y,t_{\text{FWHM}},\Delta F,\mathcal{C})}{dx dy dt_{\text{FWHM}} d\Delta F d\mathcal{C}} \right\rangle_{x^{\text{meas}}, y^{\text{meas}}, \mathcal{C}^{\text{meas}}, t_{\text{FWHM}}^{\text{meas}}, \Delta F^{\text{meas}}} &:= \\ \int \int \int \frac{d^5\Gamma(x^{\text{meas}}, y^{\text{meas}}, t_{\text{FWHM}}, \Delta F, \mathcal{C})}{dx dy dt_{\text{FWHM}} d\Delta F d\mathcal{C}} p(t_{\text{FWHM}}, t_{\text{FWHM}}^{\text{meas}}) p(\Delta F, \Delta F^{\text{meas}}) p(\mathcal{C}, \mathcal{C}^{\text{meas}}) dt_{\text{FWHM}} d\Delta F d\mathcal{C} & \end{aligned} \quad (\text{C9})$$

$$\begin{aligned} \left\langle \frac{d^6\Gamma(x,y,t_{\text{FWHM}},\Delta F,\mathcal{C},M)}{dx dy dt_{\text{FWHM}} d\Delta F d\mathcal{C} dM} \right\rangle_{x^{\text{meas}}, y^{\text{meas}}, t_{\text{FWHM}}^{\text{meas}}, \Delta F^{\text{meas}}, \mathcal{C}^{\text{meas}}} (M) &:= \\ \int \int \int \frac{d^6\Gamma(x^{\text{meas}}, y^{\text{meas}}, t_{\text{FWHM}}, \Delta F, \mathcal{C}, M)}{dx dy dt_{\text{FWHM}} d\Delta F d\mathcal{C} dM} p(t_{\text{FWHM}}, t_{\text{FWHM}}^{\text{meas}}) p(\Delta F, \Delta F^{\text{meas}}) p(\mathcal{C}, \mathcal{C}^{\text{meas}}) dt_{\text{FWHM}} d\Delta F d\mathcal{C} & \end{aligned} \quad (\text{C10})$$

Equation (C10) gives the contribution to the event rate (with event characteristics as observed) as a function of lens mass. The probability for a lens with mass M causing an observed event can therefore be written as

$$\hat{p}(M) \propto \left\langle \frac{d^6\Gamma(x,y,t_{\text{FWHM}},\Delta F,\mathcal{C},M)}{dx dy dt_{\text{FWHM}} d\Delta F d\mathcal{C} dM} \right\rangle_{x^{\text{meas}}, y^{\text{meas}}, t_{\text{FWHM}}^{\text{meas}}, \Delta F^{\text{meas}}, \mathcal{C}^{\text{meas}}} (M) \quad (\text{C11})$$

We will evaluate the lens mass probability function for each self lensing (bulge-bulge, bulge-disk, disk-disk) and halo (M31-halo-bulge, M31-halo-disk, MW-halo-bulge, MW-halo-disk) lensing scenario.

Equations C7 and C4 describe the distributions of events (at the location of the observed event) in the flux-excess-lensing time-scale plane, for the case where the observed color of the event is used (Eq. C7) and for all events,

irrespective of their color (Eq. C4). Studying the event distribution in this plane is very useful, since one can immediately see, if an event is unlikely (given a theoretical model), and how data quality (imposing limits on detectable flux excess and time scale) restricts the measurable event rate.

The relative values of Eqs. C9 and C5 give the relative probabilities for the different lensing scenarios, if the color of the event is used or not used, respectively.

We are very grateful to the anonymous referee for a lot of constructive suggestions. This research was supported by the Sonderforschungsbereich SFB 375 of the Deutsche Forschungsgemeinschaft (DFG) and by the DFG cluster of excellence Origin and Structure of the Universe (www.universe-cluster.de).

REFERENCES

- Afonso, C., Albert, J. N., Alard, C., Andersen, J., Ansari, R., Aubourg, É., Bareyre, P., Bauer, F., Beaulieu, J. P., Blanc, G., Bouquet, A., et al. 2003: *Bulge microlensing optical depth from EROS 2 observations*, A&A, 404, 145
- Alcock, C., Allsman, R. A., Alves, D. R., Axelrod, T. S., Becker, A. C., Bennett, D. P., Cook, K. H., Drake, A. J., Freeman, K. C., Geha, M., Griest, K., et al. 2001: *The MACHO Project: Microlensing Detection Efficiency*, ApJS, 136, 439
- An, J. H., Evans, N. W., Kerins, E., Baillon, P., Calchi Novati, S., Carr, B. J., Crézé, M., Giraud-Héraud, Y., Gould, A., Hewett, P., Jetzer, P., et al. 2004: *The Anomaly in the Candidate Microlensing Event PA-99-N2*, ApJ, 601, 845
- Ansari, R., Aurière, M., Baillon, P., Bouquet, A., Coupinot, G., Coutures, C., Ghesquière, C., Giraud-Héraud, Y., Gondolo, P., Hecquet, J., Kaplan, J., et al. 1999: *AgapeZ1: a large amplification microlensing event or an odd variable star towards the inner bulge of M31*, A&A, 344, L49
- Aurière, M., Baillon, P., Bouquet, A., Carr, B. J., Crézé, M., Evans, N. W., Giraud-Héraud, Y., Gould, A., Hewett, P. C., Kaplan, J., Kerins, E., et al. 2001: *A Short-Timescale Candidate Microlensing Event in the POINT-AGAPE Pixel Lensing Survey of M31*, ApJ, 553, L137
- Ballero, S. K., Kroupa, P., & Matteucci, F. 2007: *Testing the universal stellar IMF on the metallicity distribution in the bulges of the Milky Way and M 31*, A&A, 467, 117
- Brown, T. M., Ferguson, H. C., Smith, E., Kimble, R. A., Sweigart, A. V., Renzini, A., Rich, R. M., & VandenBerg, D. A. 2003: *Evidence of a Significant Intermediate-Age Population in the M31 Halo from Main-Sequence Photometry*, ApJ, 592, L17
- Calchi Novati, S., Paulin-Henriksson, S., An, J., Baillon, P., Belokurov, V., Carr, B. J., Crézé, M., Evans, N. W., Giraud-Héraud, Y., Gould, A., Hewett, P., et al. 2005: *POINT-AGAPE pixel lensing survey of M 31. Evidence for a MACHO contribution to galactic halos*, A&A, 443, 911
- de Jong, J. T. A., Widrow, L. M., Cseresnjcs, P., Kuijken, K., Crofts, A. P. S., Bergier, A., Baltz, E. A., Gyuk, G., Sackett, P. D., Ugesich, R. R., & Sutherland, W. J. 2006: *MACHOs in M31? Absence of evidence but not evidence of absence*, A&A, 446, 855
- Durrell, P. R., Harris, W. E., & Pritchett, C. J. 1994: *BR photometry of the halo of M31*, AJ, 108, 2114
- Girardi, L., Bertelli, G., Bressan, A., Chiosi, C., Groenewegen, M. A. T., Marigo, P., Salasnich, B., & Weiss, A. 2002: *Theoretical isochrones in several photometric systems. I. Johnson-Cousins-Glass, HST/WFPC2, HST/NICMOS, Washington, and ESO Imaging Survey filter sets*, A&A, 391, 195
- Gould, A., Bahcall, J. N., & Flynn, C. 1997: *M Dwarfs from Hubble Space Telescope Star Counts. III. The Groth Strip*, ApJ, 482, 913
- Griest, K. 1991: *Galactic microlensing as a method of detecting massive compact halo objects*, ApJ, 366, 412
- Kalirai, J. S., Gilbert, K. M., Guhathakurta, P., Majewski, S. R., Ostheimer, J. C., Rich, R. M., Cooper, M. C., Reitzel, D. B., & Patterson, R. J. 2006: *The Metal-poor Halo of the Andromeda Spiral Galaxy (M31)1.*, ApJ, 648, 389
- Kroupa, P. 2002: *The Initial Mass Function of Stars: Evidence for Uniformity in Variable Systems*, Science, 295, 82
- Mould, J. & Kristian, J. 1986: *The stellar population in the halos of M31 and M33*, ApJ, 305, 591
- Paczynski, B. 1986: *Gravitational microlensing by the galactic halo*, ApJ, 304, 1
- Paulin-Henriksson, S., Baillon, P., Bouquet, A., Carr, B. J., Crézé, M., Evans, N. W., Giraud-Héraud, Y., Gould, A., Hewett, P., Kaplan, J., Kerins, E., et al. 2003: *The POINT-AGAPE survey: 4 high signal-to-noise microlensing candidates detected towards M 31*, A&A, 405, 15
- Paulin-Henriksson, S. & Calchi Novati, S. 2004: *The POINT-AGAPE Microlensing Survey: First Constraint on MACHOs towards M31*, ArXiv Astrophysics e-prints
- Renzini, A. & Ciotti, L. 1993: *Transverse Dissections of the Fundamental Planes of Elliptical Galaxies and Clusters of Galaxies*, ApJ, 416, L49+
- Rich, R. M., Mighell, K. J., & Neill, J. D. 1996: *The Metal Rich Halo of M31*, in Astronomical Society of the Pacific Conference Series, Vol. 92, Formation of the Galactic Halo...Inside and Out, ed. H. L. Morrison & A. Sarajedini, 544–+
- Riffeser, A., Fliri, J., Bender, R., Seitz, S., & Gössel, C. A. 2003: *The Wendelstein Calar Alto Pixelensing Project (WeCAPP): First MACHO Candidates*, ApJ, 599, L17
- Riffeser, A., Fliri, J., Seitz, S., & Bender, R. 2006: *Microlensing toward Crowded Fields: Theory and Applications to M31*, ApJS, 163, 225
- Tisserand, P., Le Guillou, L., Afonso, C., Albert, J. N., Andersen, J., Ansari, R., Aubourg, É., Bareyre, P., Beaulieu, J. P., Charlot, X., Coutures, C., et al. 2007: *Limits on the Macho content of the Galactic Halo from the EROS-2 Survey of the Magellanic Clouds*, A&A, 469, 387
- Walterbos, R. A. M. & Kennicutt, R. C. 1987: *Multi-color photographic surface photometry of the Andromeda galaxy*, A&AS, 69, 311
- Williams, B. F. 2002: *Clues about the star formation history of the M31 disc from WFPC2 photometry*, MNRAS, 331, 293
- Zoccali, M., Cassisi, S., Frogel, J. A., Gould, A., Ortolani, S., Renzini, A., Rich, R. M., & Stephens, A. W. 2000: *The Initial Mass Function of the Galactic Bulge down to $\sim 0.15M_{\odot}$* , ApJ, 530, 418